Petrology and Geochemistry of Boninites from the North Termination of the Tonga Trench: Constraints on the Generation Conditions of Primary High-Ca Boninite Magmas

by ALEXANDER V. SOBOLEV[1] AND LEONID V. DANYUSHEVSKY[1,2]

[1]Vernadsky Institute of Geochemistry and Analytical Chemistry, Russian Academy of Sciences, Kosygin st. 19, Moscow 117975, Russia

[2]Department of Geology, University of Tasmania, GPO Box 252C, Hobart, Tasmania, 7001, Australia

ABSTRACT

We report here a detailed mineralogical, geochemical, and experimental study of a high-Ca boninite suite from the northern termination of the Tonga trench. Most samples are strongly olivine porphyritic and show a significant range of phenocryst compositions including a very refractory olivine–spinel assemblage Fo_{94}–$Cr_N = 87$. They are also characterized by a wide range of incompatible-element contents, e.g., $(La/Yb)_N$ varies from 0·5 to 16, whereas compatible major-element concentrations $(Al_2O_3, FeO, CaO, SiO_2$, and MgO) remain essentially the same. Primary melt compositions for the suite were established on the basis of an experimental study of melt inclusions in phenocrysts and numerical modelling of the reverse of fractional crystallization. Tongan primary melts are characterized by high MgO contents (22–24 wt.%) and originated in the mantle wedge at pressures of 20–25 kbar and temperatures of 1450–1550 °C. H_2O contents in primary melts were estimated from direct measurements of melt inclusions by ion probe, and range from 2·0 to 1·0 wt.%, and a strong correlation exists between H_2O and other incompatible element contents. The primary melts crystallized in the presence of an H_2O-rich fluid in the temperature range 1390–1150 °C and pressures of 1·7–0·15 kbar. Continuous degassing of melts took place during crystallization. Trace-element concentrations in primary melts were estimated using proton- and ion-probe analyses of melt inclusions in olivine, and whole-rock analyses. Our data suggest that three independent components (D, E1, and E2) were involved. Component D was a refractory mantle depleted in incompatible elements, likely to be hot 'dry' lherzolite produced by previous melting within a mantle plume. Component E1 was an H_2O-rich fluid containing LILE and Th, and had an H_2O/K_2O value of 20; it was probably produced by dehydration of the subducted slab. Component E2 is thought to have been an incompatible-element-enriched silicate melt of plume origin. Formation of high-Ca boninites requires interaction of hot 'dry' residual mantle, associated with plumes, with a subduction-related H_2O-bearing component.

INTRODUCTION

According to the recent classification of Crawford et al. (1989), the boninite series is that 'in which the volumetrically dominant lavas either have >53 wt.% SiO_2 and $Mg_N = Mg/(Mg + Fe^{2+}) > 0.6$, or are demonstrably derived from parental magmas meeting these compositional requirements'. H_2O appears to be an important component of boninitic melts (Sobolev & Danyushevsky, 1986; Bloomer & Hawkins, 1987; Dobson & O'Neil, 1987;

Offprint requests to L. V. Danyushevsky, at University of Tasmania

Sobolev *et al.*, 1993). Within the boninitic series, a separate 'high-Ca' suite, with $CaO/Al_2O_3 > 0.75$, has been recognized.

It is generally agreed that boninites are the result of melting of depleted peridotite in a mantle wedge in the presence of a hydrous fluid enriched in incompatible elements (Meijer, 1980; Hickey & Frey, 1982; Cameron *et al.*, 1983). However, compositions of primary melts and P,T conditions of their origin are not well known. Consequently, several important aspects of boninite genesis remain controversial, including the nature and composition of components involved in boninite petrogenesis, and the scenarios of component interactions in boninitic sources.

The source of compatible mantle-derived elements such as Ni, Mg, and Cr in boninites is believed to be highly refractory mantle peridotites, which are also responsible for high Si, low Al, and variable Ca in these rocks (Crawford *et al.*, 1989). The geodynamic environment in which this mantle source was formed is critical for understanding both boninite genesis and island-arc evolution in general. Following Meijer (1980), the dominant opinion is that this mantle source is essentially residual peridotite formed after extraction of N-MORB (mid-ocean ridge basalt) type magmas in a mid-ocean ridge environment. An alternative point of view was formulated by Sharaskin *et al.* (1983*a*) and Falloon & Crawford (1991), who showed that isotope geochemistry of the most depleted boninites from the northernmost Tonga trench indicate an ocean island basalt (OIB) type nature for their mantle reservoir. If true, this interpretation could more closely constrain the origin of boninites and imply a close connection with mantle plumes. However, Stern *et al.* (1991) argued that Nd–Sm, Rb–Sr, and Pb–U isotopic data for boninites provide information only on the enriched components, even for the most depleted varieties, and thus do not provide any information on the nature of their mantle-derived component.

The nature of enriched component(s) in boninite sources is generally related to subduction processes. The following enriched components have been proposed to take part in boninite genesis: fluids from the subducted slab (Meijer, 1980), silicate melt, either from the slab or from the mantle wedge (Hickey & Frey, 1982; Pearce *et al.*, 1992), and ephemeral carbonatitic melt (Falloon & Crawford, 1991). However, the exact composition and the number of components are not well known and differ between localities (Crawford *et al.*, 1989).

Two contrasting models can be put forward to describe boninite petrogenesis. The first argues for boninite generation by reheating of cold, metasomatized H_2O-bearing mantle (Crawford *et al.*, 1989). The second suggests melting of relatively hot, depleted dry mantle during metasomatism by H_2O-bearing fluids (Meijer, 1980). These models have different consequences for the modelling of boninite genesis. The latter requires a very hot mantle wedge but no extra heating for melting. The former involves normal sub-arc mantle, but needs a mechanism of extra heating, such as subduction of a spreading centre (Crawford *et al.*, 1989).

In this paper, we present new experimental, mineralogical, and geochemical data for high-Ca boninites from the north Tonga trench and use these, together with other published data (Sharaskin *et al.*, 1983*b*; Falloon *et al.*, 1989; Falloon & Crawford, 1991) to determine the composition of primary melts (including H_2O content) and the P,T conditions of their formation. We show that the primary magmas of these high-Ca boninites, with >21 wt.% MgO, require very high temperatures ($\sim 1500\,°C$), segregated around 20–25 kbar, and have relatively low H_2O content (~ 2 wt.%) compared with 5–7 wt.% H_2O suggested from high-pressure experiments on boninite petrogenesis (Umino & Kushiro, 1989; Van der Laan *et al.*, 1989). Our data suggest that petrogenesis of these high-Ca boninites requires mixing of an H_2O-bearing slab-derived component with hot, dry OIB-type mantle.
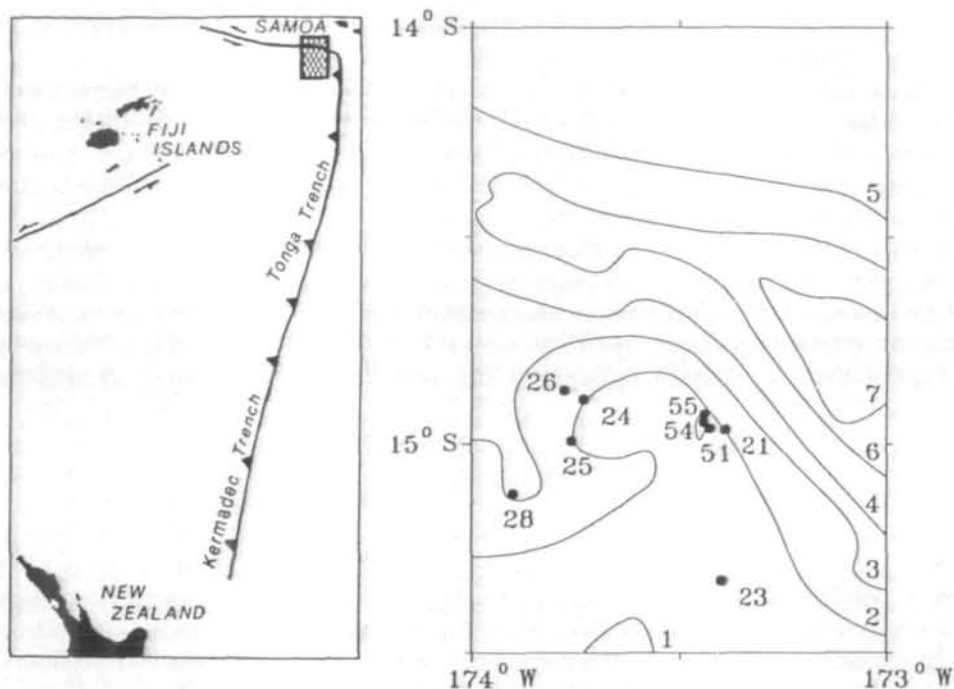
FIG. 1. Schematic locality map of the northern termination of the Tonga trench after Sharaskin *et al.* (1983*b*) and Falloon & Crawford (1991), showing locations of boninite-bearing dredges. Depths in kilometres.

SAMPLE LOCATIONS

Boninites were dredged from the inner slope of the Tonga trench close to its northern termination during cruise 16 of R/V *Kallisto* in 1982 [stations 26 (samples 26-1 and 26-2), 28 (sample 28-1), and 51, Sharaskin *et al.* (1983*b*)] and a cruise of R/V *Natsushima* in 1984 [stations 21 (sample 3-44), 23 (samples 5-24, 5-25, and 5-28), 24 (sample 6-3), and 25 (sample 7-18), Falloon *et al.* (1987)] (Fig. 1). The dredge stations are divided into two groups according to their location—Western stations 24, 25, 26, and 28, and Eastern stations 21, 23, and 51. Also dredged from these areas were serpentinites, gabbros [some with boninitic affinities (Sharaskin *et al.*, 1983*b*)], and doleritic dykes.

ANALYTICAL TECHNIQUES

Whole-rock compositions were obtained by X-ray fluorescence (XRF) spectrometry at Vernadsky Institute, Moscow, using a Phillips PW-1400 spectrometer, by inductively coupled plasma atomic emission spectrometry (ICP AES) at CRPG, Nancy, France (Govindaraju & Mevelle, 1987), and by instrumental neutron activation analysis (INAA) at Pierre Sue Laboratory, Saclay, France (Chayla *et al.*, 1973).

Minerals and glasses were analysed at the Vernadsky Institute with a CAMEBAX MicroBeam electron microprobe and at the University of Tasmania with a CAMECA SX/50 microprobe, using 15 kV accelerating voltage and 20 nA beam current. Counting time was 10 s. The beam diameter was 1–2 μm for minerals and 10 μm for glasses. Clinopyroxenes USNM 122142, plagioclase USNM 115900, basalt glass USNM 111240/52 (Jarosewich *et*

al., 1980), olivine CH-1, and spinel UV-126 (Lavrentev *et al.*, 1974) were used as standards for major elements.

Trace elements in melt inclusions were analysed by an IMS-3F ion microprobe at Massachusetts Institute of Technology, Cambridge, and by proton microprobe at the Commonwealth Scientific and Industrial Research Organisation, Sydney, Australia. Technique details have been given by Shimizu & Hart (1982) and Sie *et al.* (1990). Accuracy of both methods is considered to be 10–20 rel.%.

The molecular composition of fluid inclusions in olivine was obtained using Raman spectroscopy at high temperatures (Sobolev *et al.*, 1983) at CREGU, Nancy, France.

H_2O contents were measured in quenched glasses and melt inclusions by Fourier transform infra-red spectroscopy (Danyushevsky *et al.*, 1993) and an ion microprobe technique (Sobolev & Chaussidon, in prep.). The accuracy of both methods is estimated to be better than 10 rel.%.

PETROGRAPHY AND MINERALOGY

The petrography of the Tongan boninites was presented in detail elsewhere (Sharaskin *et al.*, 1983*b*; Falloon *et al.*, 1987; Visotsky, 1989). Most samples studied in this paper are strongly porphyritic and contain up to 50% phenocrysts, which are euhedral prismatic olivine crystals typically 1–10 mm long. Small (up to 3 mm long) phenocrysts of ortho- and clinopyroxene are also present. Groundmass consists of glass with variable amounts of olivine and pyroxene microphenocrysts and microlites. Spinels are present as inclusions in all phenocryst phases, but rarely occur as discrete crystals. Sample 28-1 is a volcanic glass with rare microphenocrysts of orthopyroxene, plagioclase, and magnetite. Rare microlites consist of the same minerals. There is no petrographic evidence for secondary alteration in the boninite samples studied.

The following types of primary inclusions in minerals have been identified in the samples studied [see Roedder (1984) for inclusion classification]: (1) glassy and partially crystallized melt inclusions in olivine, pyroxenes, and spinel; (2) fluid inclusions in olivine, pyroxenes, and groundmass glasses; (3) crystalline inclusions in olivine (spinel), orthopyroxene (spinel, clinopyroxene), and clinopyroxene (spinel, olivine); (4) multi-phase inclusions, abundant in all minerals and represented mainly by combinations of glass + spinel, glass + fluid, and glass + fluid + spinel.

Phenocryst mineralogy

Olivine

Olivine crystals in all samples are unzoned and very magnesian, up to Fo_{93} for the Western group and up to Fo_{94} for the Eastern group (Fig. 2, Table 1). A coherent CaO vs. Fo trend (Fig. 2), which is more Ca rich than that of mantle olivines [CaO < 0·1 wt.%, Simkin & Smith (1980)], and the presence of melt inclusions suggest that olivines in these rocks, including the most magnesian crystals, crystallized from the boninite magma and are not xenocrysts of mantle origin. Histograms of Fo content (Fig. 2) show a unimodal distribution for the Western group boninites, and a bimodal distribution for the Eastern group. The range of Fo contents of the Tongan olivines is similar to that of boninites in general, and they are among the most Ca-rich olivines so far analysed from boninites.

Spinel

Spinels show a wide range of compositions. The Western group spinels are characterized
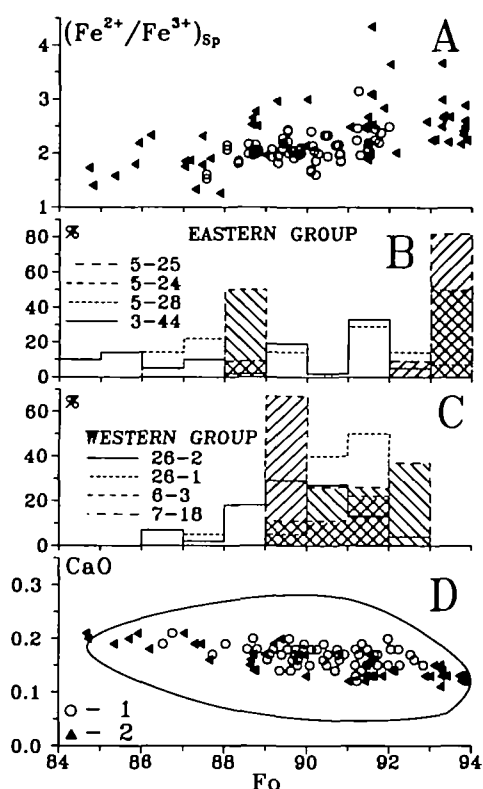
FIG. 2. Olivine phenocrysts from Tongan high-Ca boninites. 1, Western group olivines; 2, Eastern group olivines; A, relationship between host olivine composition and Fe^{2+}/Fe^{3+} of spinel inclusions; B, C, composition histograms for four samples from each group; D, CaO content; general boninite field after Kuroda et al. (1978), Crawford (1980), Walker & Cameron (1983), Cameron (1985), Crawford & Cameron (1985), Bloomer & Hawkins (1987), Falloon et al. (1989), and our unpublished data.

by relatively lower Cr_N [$Cr/(Cr+Al)$], and higher Mg_N and TiO_2 contents than the Eastern group spinels (Fig. 3, Table 1). Spinels with $Fe^{2+}/Fe^{3+} > 3$ are absent in the Western group. In both groups the large range of TiO_2 contents in spinels in each sample cannot have been produced during simple fractional crystallization. Tongan high-Ca boninite spinel populations do not contain the Cr-rich spinels ($Cr_N > 88$) present in low-Ca boninites. However, they cover the total range of boninitic spinel TiO_2 contents and Fe^{2+}/Fe^{3+} values.

Pyroxenes

Phenocryst compositions from sample 26-2 are listed in Table 1. Orthopyroxenes resemble those from other boninites, whereas clinopyroxene compositions are characterized by higher Mg_N and Cr_2O_3 contents (Kuroda et al., 1978; Crawford, 1980; Peive, 1980; Walker & Cameron, 1983; Ohnenstetter & Brown, 1992). Mg_N values of Tongan orthopyroxenes range from 90 to 87, and those for clinopyroxenes range from 91 to 86.

CHEMISTRY

Fluid composition

The maximum size of primary fluid inclusions in olivines is $\sim 150\,\mu m$. Most of the volume of individual inclusions is composed of a gas phase; a liquid phase occurs as a film on

TABLE 1

Compositions of crystalline inclusions in phenocrysts from the Western group Tongan boninites

Sample	26-2													26-1						28-1
No.	O-32	O-12	O-65	O-51	O-62	O-40	Op-29	Op-6	Op-9	Cp-6	Cp-10	Op-42	Cp-4	OL-8	OL-37	OL-32	OL-1	OL-11	OL-9	Op-1
HOST	Ol	Ol	Ol	Ol	Ol	Ol	Opx	Opx	Opx	Cpx	Cpx	Opx	Cpx	Ol	Ol	Ol	Ol	Ol	Ol	Opx
SiO_2	41·31	40·67	40·48	40·16	40·92	40·41	55·88	57·57	56·35	53·72	54·04	56·39	54·13	40·88	40·54	40·54	40·68	40·39	40·36	52·42
TiO_2	—	—	—	—	—	—	0·06	0·04	0·04	0·11	0·13	0·08	0·14	—	—	—	—	—	—	0·17
Al_2O_3	—	—	—	—	—	—	0·72	0·67	0·66	1·60	1·55	1·00	1·28	—	—	—	—	—	—	0·97
$FeO*$	7·83	8·34	9·15	9·63	9·81	11·57	6·70	7·23	8·01	4·33	4·59	8·11	4·05	8·20	8·46	8·46	9·05	9·56	10·02	23·00
MnO	0·14	0·15	0·12	0·16	0·15	0·17	0·17	0·25	0·21	0·11	0·15	0·14	0·12	0·13	0·12	0·15	0·12	0·14	0·16	0·67
MgO	50·59	50·20	48·99	48·28	47·86	47·75	33·86	32·68	32·27	19·15	19·33	32·26	19·19	50·44	49·36	49·10	49·39	48·71	48·68	21·48
CaO	0·17	0·18	0·17	0·18	0·17	0·19	1·76	2·07	2·16	19·37	19·01	1·92	20·04	0·17	0·12	0·15	0·17	0·15	0·17	1·93
Na_2O	—	—	—	—	—	—	0·02	0·02	0·03	0·15	0·15	0·01	0·14	—	—	—	—	—	—	0·03
Cr_2O_3	0·10	0·10	0·00	0·00	0·00	0·06	0·40	0·33	0·26	0·71	0·77	0·39	0·68	0·12	0·14	0·28	0·10	0·07	0·07	0·03
NiO	0·22	0·27	0·14	0·18	0·19	0·21	—	—	—	—	—	—	—	0·37	0·25	0·29	0·30	0·23	0·20	0·04
Mg_N	92·0	91·5	90·5	89·9	89·7	88·0	90·0	89·0	87·8	88·8	88·2	87·64	89·42	91·64	91·23	91·19	90·68	90·08	89·65	37·50
INCL.	Sp	Sp	Sp	Sp	Sp	Sp	Sp	Sp	Sp	Sp	Sp	Cpx	Ol-1	Ol-2	Sp	Sp	Sp	Sp	Sp	Pl
SiO_2	0·11	0·13	0·10	0·12	0·23	0·11	0·00	0·00	0·11	0·00	0·15	52·41	40·20	40·51	0·07	0·08	0·06	0·08	0·06	48·66
TiO_2	0·29	0·30	0·28	0·27	0·33	0·35	0·30	0·30	0·42	0·44	0·69	0·16	—	—	0·18	0·09	0·20	0·24	0·10	0·28
Al_2O_3	8·42	8·26	8·77	8·16	8·05	9·02	9·31	9·80	10·65	9·80	10·23	1·80	—	—	7·65	6·63	7·70	7·73	7·29	32·08
$FeO*$	17·59	17·89	20·05	21·27	21·89	23·53	24·06	24·65	27·91	24·65	26·60	4·47	12·03	11·71	17·42	20·54	18·53	20·03	21·80	1·68
MnO	0·17	0·13	0·22	0·24	0·20	0·26	0·19	0·27	0·25	0·27	0·23	0·10	0·22	0·19	0·19	0·23	0·19	0·19	0·15	—
MgO	14·34	14·18	13·43	12·27	12·11	11·47	11·60	11·34	10·70	11·34	10·76	18·47	47·12	47·13	13·68	11·38	13·38	12·78	11·28	—
CaO	—	—	—	—	—	—	—	—	—	—	—	19·37	0·18	0·34	—	—	—	—	—	15·73
Na_2O	—	—	—	—	—	—	—	—	—	—	—	0·13	—	—	—	—	—	—	—	2·33
Cr_2O_3	58·35	58·78	57·14	55·93	56·25	54·39	51·77	50·94	47·90	50·94	47·22	0·72	0·00	0·03	60·70	60·81	59·86	58·25	57·20	—
V_2O_3	0·12	0·16	0·20	0·16	0·18	0·19	0·20	0·28	0·21	0·28	0·22	—	—	—	0·37	—	0·29	0·30	0·23	—
a	1·94	2·06	1·95	2·08	2·22	2·16	1·63	1·72	1·61	1·80	1·70	88·05	87·47	87·77	2·45	3·15	2·21	2·16	2·41	78·90
T (°C)	1290	—	1255	1250	1235	—	—	1170	1150	—	—	—	—	—	—	—	—	—	—	—

No.—inclusion number; HOST—the type of the host phenocryst (Op-1 microphenocryst); INCL.—the type of crystalline inclusion; $a = Fe^{2+}/Fe^{3+}$ for spinel (calculated on the basis of stoichiometry); $a = Mg_N$ for olivine and pyroxenes; a = An for plagioclase; T—the temperature of phenocryst crystallization, obtained from the melt-inclusion study; Ol—olivine, Opx—orthopyroxene, Cpx—clinopyroxene, Sp—spinel, Pl—plagioclase.
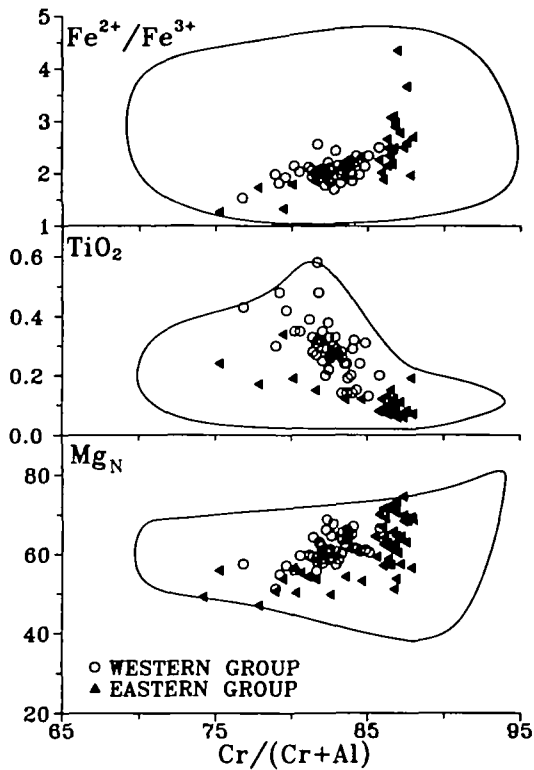
FIG. 3. Spinel inclusions in phenocrysts from the Tongan high-Ca boninites. General boninite field after Kuroda *et al* (1978), Crawford (1980), Walker & Cameron (1983), Cameron (1985, 1989), Crawford & Cameron (1985), Bloomer & Hawkins (1987), Falloon *et al.* (1989), and our unpublished data. Fe^{3+} was calculated according to stoichiometry.

inclusion walls and can be seen only during heating at temperatures $> 200\,^{\circ}C$ by the movement of mineral particles. The main component of the fluid is H_2O. CO_2 is present in trace amounts (~ 0.1 mol%). Other components, notably CO and CH_4 were not detected. In quenched glasses, fluid inclusions at room temperature also consist mainly of a gas phase, but a liquid phase is visible. Sobolev & Danyushevsky (1986) demonstrated the magmatic nature of these inclusions. The presence of primary H_2O-rich fluid inclusions in all phases of Tongan boninites argues for H_2O saturation of the melt during the entire course of its crystallization history.

Major elements

Rocks and glasses

The compositions of glasses and rocks (Tables 2 and 3) are plotted in Fig. 4 together with available data for whole-rock, groundmass, and glass compositions from the Tongan boninites. Significant differences exist in FeO*, K_2O, and P_2O_5 contents between the Western and Eastern group boninites (Fig. 4), the Western group being characterized by generally lower FeO* and higher K_2O and P_2O_5. Broad variations within each group in the contents of the most incompatible elements (TiO_2, P_2O_5, and K_2O) at constant MgO content cannot be explained by fractionation, and appear to reflect the variable composition

TABLE 2

Compositions of quenched glasses

Sample	26-2	26-1	28-1	26-3	6-2	6-3	7-18	5-25	5-25a
SiO$_2$	59·93	56·73	66·50	56·93	57·36	57·18	56·05	54·23	57·29
TiO$_2$	0·53	0·27	0·59	0·29	0·39	0·25	0·53	0·47	0·31
Al$_2$O$_3$	16·01	13·86	12·90	13·95	12·31	11·70	11·84	13·11	13·00
FeO*	7·47	7·87	7·82	7·95	7·75	7·87	8·10	10·01	8·90
MnO	0·11	0·12	0·13	0·12	0·15	0·11	0·15	0·19	—
MgO	2·71	6·29	1·48	6·35	7·67	8·62	8·37	5·83	8·80
CaO	7·14	11·03	5·48	10·95	10·49	10·15	10·54	10·78	9·90
Na$_2$O	2·1	1·33	2·51	1·30	1·40	1·38	1·76	1·76	1·50
K$_2$O	0·68	0·39	1·04	0·39	0·50	0·47	0·78	0·20	0·20
P$_2$O$_5$	—	0·02	0·17	0·03	0·06	0·06	0·26	0·00	—
Cr$_2$O$_3$	—	0·04	0·00	0·05	0·05	0·09	0·10	0·04	—
H$_2$O†	—	1·7	1·7	1·6	1·6	1·4	1·3	—	—
H$_2$O‡	—	1·4	—	—	—	—	—	1·0	—
Total	96·24	99·65	100·32	99·91	99·73	99·28	99·78	97·62	100
Mg$_N$	39·28	58·76	25·23	58·75	63·82	66·13	64·82	50·94	63·81

5-25a—the composition of groundmass determined by electron microprobe broad-beam area scans, analysis from Falloon *et al.* (1989).

* Total iron as FeO.

† Measured by IR spectroscopy.

‡ Measured by ion microprobe.

of primary melts. However, the tight trends of SiO$_2$, Al$_2$O$_3$, CaO and FeO* vs. MgO indicate that major-element compositions of these primary melts were probably fairly similar.

Melt inclusions

To determine the melt composition at various stages of its crystallization history, together with temperature of crystallization, a heating stage study of melt inclusions in olivines and orthopyroxenes from the Western group sample 26-2 was carried out (see Appendix A for the details of technique). Sixty runs were done with inclusions in olivine, and five with inclusions in orthopyroxene. Homogenization of melt inclusions was established in 15 runs with olivine, and in every run with orthopyroxene. The range of homogenization temperatures of inclusions in olivines is 1230–1330 °C; in orthopyroxenes it is 1150–1185 °C.

The correlation between the composition of a mineral and its crystallization temperature (correlation coefficient $r = 0.70$), a feature demanded by fractional crystallization, is shown in Fig. 5b. Temperatures obtained for orthopyroxene are in agreement with those calculated using two-pyroxene equilibria [Lindsley (1983), Fig. 5a]. For reasons given in Appendix A, experiments with the lowest homogenization temperatures at a fixed mineral composition were deemed to be most useful and correct. Compositions of quenched inclusions homogenized during these runs are listed in Table 4.

Compositions of homogenized melt inclusions from sample 26-2 fall within the field of rocks and natural glasses of the Western group (Fig. 4). The only observed difference is systematically lower FeO* concentrations in the melt inclusions in olivine (Fig. 4). $K_D(Fe^{2+}-Mg)$ values between host olivine and melt inclusion of 0·36–0·39 (Table 4) are significantly higher than those measured experimentally for dry and H$_2$O-bearing systems [0·3 ± 0·03 (Roeder & Emslie, 1970; Ulmer, 1989)]. The high Mg$_N$ values and low FeO* contents of these inclusions together argue for the re-equilibration of Fe^{2+} and Mg between

<div align="center">

TABLE 3

</div>

Major- and trace-element concentrations in high-Ca boninites (wt. % and ppm, respectively)

Sample	Western group				Eastern group				PM	CH
	26-1	26-2	6-3	7-18	5-24	5-28	5-25	3-44		
SiO₂	53·78	47·90	56·04	54·72	52·95	53·72	53·83	54·35	—	—
TiO₂	0·22	0·20	0·31	0·45	0·15	0·14	0·36	0·20	—	—
Al₂O₃	10·64	5·99	10·60	10·90	7·92	8·27	9·63	10·67	—	—
FeO*	8·28	9·76	8·46	8·65	9·70	9·65	9·71	9·41	—	—
MnO	0·15	0·17	0·17	0·17	0·21	0·20	0·19	0·19	—	—
MgO	13·66	28·35	13·61	12·97	20·89	19·65	16·30	14·99	—	—
CaO	8·58	4·90	9·17	9·65	7·18	7·54	8·50	8·66	—	—
Na₂O	1·04	0·77	1·14	1·52	0·85	0·69	1·27	1·14	—	—
K₂O	0·29	0·30	0·43	0·71	0·14	0·12	0·16	0·35	—	—
P₂O₅	0·06	0·06	0·07	0·26	0·01	0·02	0·04	0·03	—	—
LOI	1·53	0·35	1·87	1·69	0·13	0·00	0·24	0·05	—	—
Total	98·23	99·17	100	100	100	100	100	100	—	—
Cr	971	2183	927	760	2027	1667	1294	1095	—	—
Ni	266	732	189	199	501	433	341	275	—	—
Co	44	83	—	—	—	—	—	—	—	—
Sc	40·0	24·5	43	44	44	43	44	50	—	—
V	195	119	214	223	191	200	225	247	—	—
Cs	0·167	0·116	—	—	—	—	—	—	0·008	—
Rb	5·60	5·96	8	12	2	2	3	6	0·635	—
Ba	58·0	64·4	105	230	34	35	41	106	6·989	—
Th	0·583	0·656	1·14	2·42	0·24	—	—	0·48	0·085	—
U	0·168	0·164	—	—	—	—	—	—	0·021	—
K†	2408	2491	3570	5894	1162	3985	1328	2906	250	—
Sr	98	87	159	348	46	48	68	151	21·1	—
Ta	0·226	0·264	—	—	—	—	—	—	0·041	—
Nb	—	—	8	16	—	—	—	—	0·713	—
P†	262	262	305	1135	44	218	175	131	95	—
Zr	24	26	32	53	—	7	20	—	11·2	—
Hf	0·487	0·475	0·93	1·7	0·33	—	—	0·61	0·309	—
Ti†	1319	1200	1859	2698	900	1859	2159	1199	1300	—
Y	7	6	8	11	5	6	10	7	4·550	—
La	3·06	3·82	6·53	15·98	0·41	—	1·51	1·77	0·687	0·367
Ce	6·03	7·40	14·74	37·72	1·00	—	3·34	4·10	1·775	0·957
Pr	—	—	1·73	4·48	—	—	0·55	—	0·276	0·137
Nd	—	—	6·36	17·29	0·90	—	2·72	2·85	1·354	0·711
Sm	0·696	0·784	1·30	3·23	0·40	—	0·89	0·82	0·444	0·231
Eu	0·237	0·283	0·45	1·02	—	—	0·36	—	0·168	0·087
Gd	—	—	1·35	2·68	0·69	—	1·27	1·27	0·596	0·306
Tb	0·124	0·094	—	—	—	—	—	—	0·108	0·058
Dy	—	—	1·27	1·84	0·87	—	1·62	1·16	0·737	0·381
Er	—	—	0·63	0·93	0·57	—	1·10	0·80	0·480	0·249
Yb	0·776	0·630	0·58	0·79	0·71	—	1·14	0·86	0·493	0·248

26-1 and 26-2 are our data; others are from Falloon *et al.* (1989), Falloon & Crawford (1991).

* Total iron as FeO.

† Recalculated from the major-element analyses.

PM—primitive mantle (Sun & McDonough, 1989); CH—chondrite (Tayor & McLennan, 1981). Cr, Ni, V, Sr, Zr, and Y in samples 26-1 and 26-2 were analysed by ICP, other trace elements by INAA

the inclusions and the host olivines after trapping (Gurenko *et al.*, 1991). To achieve the initial equilibrium between melt inclusion and host olivine, the redistribution of Fe into inclusions and Mg into host olivines can be calculated using equations of Ford *et al.* (1983). The calculated compositions are listed in Table 4, and FeO contents of the recalculated melts correspond to the field of rocks and glasses (Fig. 4).

Results obtained for sample 26-2 demonstrate the evolution of Western group melts during crystallization within the temperature range 1300–1150 °C, which corresponds to ~30% of fractionation (Table 4).
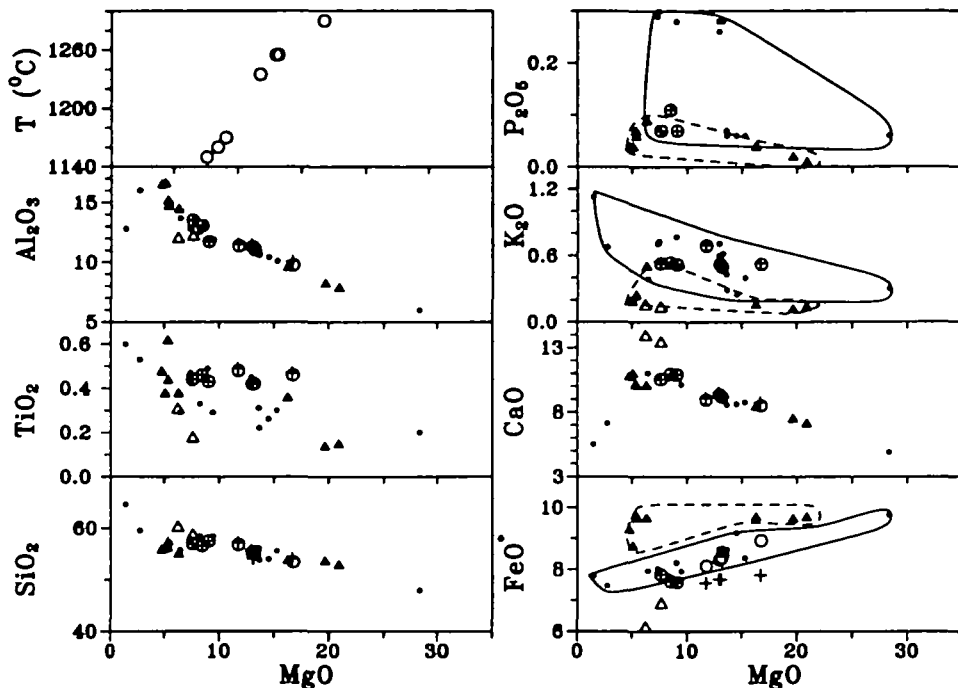
FIG. 4. Composition of rocks, natural glasses, and homogenized melt inclusions from Western and Eastern groups of the Tongan boninites. Data from this study and Sharaskin *et al.* (1983*b*), Falloon *et al.* (1987, 1989), and Falloon & Crawford (1991). ●, Western group rocks; ▲, Eastern group rocks; +, homogenized melt inclusions; ○, compositions of homogenized melt inclusions corrected for Fe–Mg exchange with host mineral (see text for discussion); △, compositions of naturally quenched melt inclusions in olivine Fo_{94} from the Eastern group, used by Falloon & Green (1986) for calculation of primary melt composition.

H_2O content

The data (Tables 2 and 4) show that H_2O contents in naturally quenched melt inclusions are significantly higher than those in quenched volcanic glasses. The former are trapped primitive melts, affected by olivine crystallization on the walls (15–30%, Table 4), whereas the latter are the result of > 30% of fractional crystallization of these melts (see the above paragraph). The data show the degassed nature of Tongan glasses and relatively undegassed H_2O contents of inclusions, and argue for a significant loss of H_2O from the melt during crystallization. This is also supported by the H_2O content of homogenized melt inclusions, which represent primitive melts without significant crystallization, but have H_2O contents equal to or even higher than evolved glasses. Magma degassing is directly supported by the presence of H_2O-rich fluid inclusions in olivines and glasses.

Trace elements

Trace-element concentrations are listed in Tables 3 and 5. A comparison of chondrite-normalized REE patterns between whole rocks and melt inclusions for samples 26-1 and 26-2 (Fig. 6) demonstrates a general similarity of pattern shapes for inclusions and host rocks. This suggests that, at least for the studied samples, inclusions are representative of melt composition not only in terms of major elements, but trace elements as well. The observed difference in the absolute concentration of REE in melt inclusions and in the whole-rock for sample 26-2 is due to the phenocryst-rich nature of the rock. Ratios between large ion
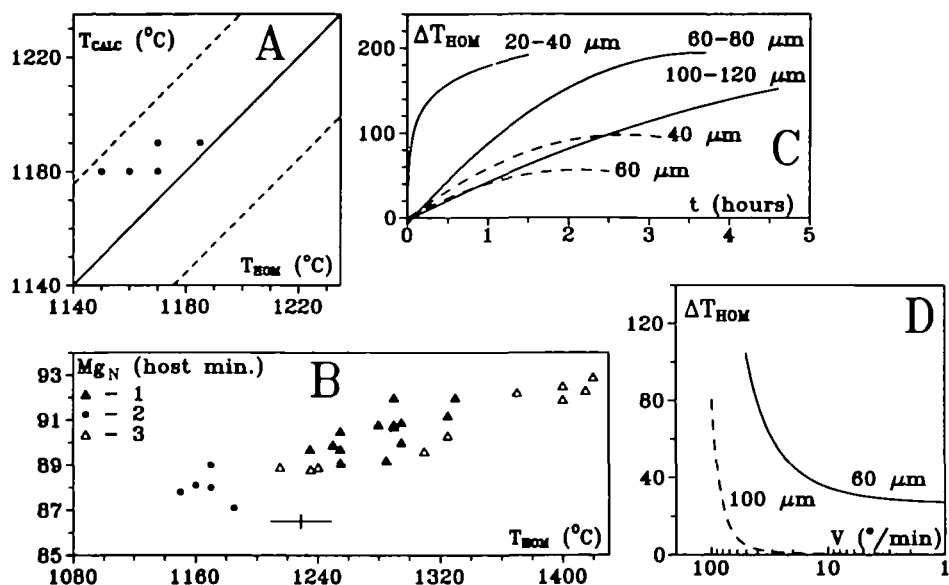
FIG. 5 Homogenization temperatures of melt inclusions in olivines and orthopyroxenes from sample 26-2. A, comparison of homogenization temperatures of inclusions in pyroxenes with temperatures, calculated from host-mineral compositions using two-pyroxene thermometer of Lindsley (1983); dashed lines indicate the accuracy of the two-pyroxene thermometer. B, correlation between homogenization temperatures and host-mineral composition. The elongate cross shows error bars for B. 1, Tongan olivines; 2, Tongan orthopyroxenes; 3, olivines from Troodos high-Ca boninite UPL. The correlation between olivine compositions and its crystallization temperature fits well to that demonstrated by Sobolev *et al.* (1993) for Troodos high-Ca boninites. C, D, the correlation of homogenization temperature with heating velocity and run duration. ΔT_{HOM} is the difference between experimentally obtained homogenization temperature and true homogenization temperature for melt inclusions; numbers in μm represent inclusion size; in C solid lines stand for olivine, dashed lines for orthopyroxene; in D solid line stands for melt inclusions in MORB olivines, dashed line for inclusions in Tongan olivines. Comparison with MORB (D, our unpublished data) shows relatively low viscosity and, respectively, high velocity of processes in boninite melts.

lithophile elements (LILE) Rb, Ba, K, and Sr, and REE, are reasonably close for rocks and melt inclusions in olivines for the same samples. This indicates that whole-rock LILE concentrations are not affected by post-magmatic processes.

The normalized REE patterns of the rocks and the melt inclusions of the Tongan boninites are plotted in Fig. 6. Whereas the Western group boninites are characterized by V-shaped or enriched REE patterns with very high La/Sm values [$(La/Sm)_N = 3-4$], the Eastern group rocks have slightly enriched or depleted patterns. The absolute REE concentrations vary significantly, and mimic the behaviour of Ti, K, and P. Other aspects of trace-element geochemistry are discussed in the following sections.

PRIMARY MELTS

We consider primary melt as a melt which has not undergone any compositional changes since the moment of its last equilibrium with the mantle source. Parental melt is the least-evolved melt which can be established from a study of the products of crystallization (rocks, quenched glasses, minerals, etc.).

Parental melt composition

True fractional crystallization of high-Ca boninites implies that the melt which was in equilibrium with the most magnesian olivine is the parental melt for the entire series. The

TABLE 4

Compositions of the melt inclusions in minerals

Locality	Western group												Eastern group			
Sample	26-2											26-1	5-25			
	H	C	H	H	C	H	C	H	H	H	H	U	U	U	U	U
No.	1	2	3	4	5	6	7	8	9	10	11	12	13	14	15	16
	O-32	O-32	O-65b	O-65a	O-65	O-62	O-62	Op-6	Op-10	Op-9	O-43	O-1	3	4	5	y
T_{HOM}	1290	1290	1255	1255	1255	1235	1235	1170	1160	1150	1330	—	—	—	—	—
Host	Ol	Ol	Ol	Ol	Ol	Ol	Ol	Op	Op	Op	Ol	Ol	Ol	Ol	Ol	Ol
SiO_2	52·70	52·35	54·06	53·89	54·51	55·81	55·96	56·18	55·08	55·51	51·22	56·55	55·74	57·89	57·80	58·08
TiO_2	0·46	0·45	0·41	0·41	0·41	0·48	0·47	0·42	0·45	0·43	0·31	0·28	0·17	—	0·30	0·26
Al_2O_3	9·83	9·58	10·92	11·11	10·89	11·27	11·21	11·46	12·73	13·17	9·07	12·19	11·64	12·75	11·57	12·91
FeO^*	7·61	8·75	7·39	7·44	8·27	7·38	7·98	7·42	7·41	7·67	7·77	7·40	6·55	4·57	5·89	5·23
MnO	0·19	0·19	0·12	0·18	0·12	0·14	0·14	0·15	0·13	0·22	0·11	0·16	—	—	—	0·09
MgO	16·26	16·42	12·68	12·56	13·02	11·44	11·59	8·86	8·24	7·40	17·64	6·02	7·23	4·79	5·99	3·85
CaO	8·55	8·34	9·10	9·23	9·08	8·87	8·83	10·67	10·68	10·28	8·07	10·91	12·77	14·05	13·39	13·16
Na_2O	1·17	1·14	1·53	1·41	1·53	1·45	1·44	1·78	1·85	1·99	1·19	1·48	0·59	0·81	0·69	1·13
K_2O	0·52	0·51	0·49	0·51	0·49	0·68	0·68	0·51	0·53	0·52	0·41	0·29	0·13	0·17	0·15	0·21
P_2O_5	—	—	—	—	—	—	—	0·07	0·11	0·07	0·08	—	—	—	—	0·07
Cr_2O_3	0·15	0·15	0·07	0·07	0·07	0·09	0·09	0·10	0·07	0·07	0·10	—	—	—	—	0·07
Total	97·43	98	96·76	96·91	98·5	97·61	98·5	97·62	97·28	97·33	95·97	95·33	94·83	95·03	95·79	94·99
H_2O	—	—	1·8	1·4	1·6	1·4	1·4	—	—	—	1·4	2·4	3·5	2·5	3·5	2·8
FeO	6·74	7·71	6·51	6·56	7·24	6·47	6·97	6·48	6·44	6·65	6·93	—	—	—	—	—
Fe_2O_3	0·96	1·16	0·97	0·98	1·14	0·99	1·12	1·04	1·08	1·13	0·93	—	—	—	—	—
Mg_N	81·1	79·2	77·6	77·3	76·2	75·9	74·8	70·9	69·5	66·5	81·9	—	—	—	—	—
$Mg_{N,w}$	92·0	92·0	90·5	90·5	90·5	89·7	89·7	89·0	88·1	87·8	92·0	89·9	94·0	94·0	94·0	94·0
K_D	0·37	0·33	0·36	0·36	0·33	0·36	0·33	—	—	—	0·39	—	—	—	—	—
T_cOl	1385	—	1324	1319	—	1299	—	1232	1216	1195	1414	—	—	—	—	—
Ol	—	—	—	—	12·0	—	14·2	20·0	20·0	20·9	—	—	—	—	—	—
Opx	—	—	—	—	—	—	—	—	3·3	2·8	—	—	—	—	—	—
Cpx	—	—	—	—	—	—	—	—	—	3·9	—	—	—	—	—	—
Diff.	—	—	—	—	0·08	—	0·85	0·29	0·20	0·17	—	—	—	—	—	—
% Ol	—	—	—	—	—	—	—	—	—	—	—	16·1	27·9	22·6	27·6	30·8

H — homogenized melt inclusions; C — recalculated compositions; U – unheated (naturally quenched) melt inclusions: 1, 3, 4, 6, 8–10 — homogenized melt inclusions in phenocrysts from the most successful runs (see text), 2, 5, 7 — melt composition calculated from composition of corresponding homogenized melt inclusions in olivine by Fe–Mg exchange (see text for details), 11 — homogenized melt inclusion, major-element compositions of inclusions 13–15 are from Falloon & Green (1986); No — unique inclusion number. T_{HOM} — homogenization temperature. Host — type of the host mineral. FeO^* — total iron as FeO. H_2O measured using ion microprobe; FeO and Fe_2O_3 calculated using spinel compositions in the same host minerals after Maurel & Maurel (1982a); $Mg_{N,w}$ — composition of the host-mineral; K_D for Fe–Mg partitioning between olivine and melt; T_cOl — calculated temperature of 'dry' 1 atm liquidus of olivine using equations of Ford et al. (1983), assuming all Fe as FeO; Ol, Opx, and Cpx — percent of mineral amounts which have crystallized from the most primitive melt (O-32) to the given composition, obtained by mixing calculations using a least-squares method (Wright & Doherty, 1970), these are calculated for homogenized inclusion only; Diff — calculation error, i.e., the sum of squares of residuals. %Ol — the calculated amount of olivine (wt %) crystallized from trapped melt on the walls of inclusions estimated by modelling of the reverse of olivine crystallization up to equilibrium with the host olivine, this was calculated for unheated inclusions only; olivine–melt equilibria during calculations were calculated after Ford et al. (1983).

TABLE 5

Trace-element concentrations in melt inclusions

Sample	26-2					26-1
No.	O-32	O-65b	O-65a	Op-9	O-43	O-1
Cr	—	—	—	—	782	481
Rb	8·0	7·4	7·5	8·4	8·2	—
Ba	90·6	—	—	92·8	—	—
Sr	143	183	163	216	129	84·7
Nb	5·6	9·1	7·3	10·1	5·6	4·24
Zr	30·1	39	30	36·9	24	27·8
Ti	—	2104	2049	—	1847	1514
Y	6·5	7	7	6·7	6	5·4
La	—	8·33	6·53	—	7·50	4·59
Ce	—	17·62	13·50	—	14·60	7·70
Nd	—	9·38	6·71	—	7·59	3·31
Sm	—	1·87	1·37	—	1·76	0·89
Dy	—	1·87	1·61	—	1·59	0·92
Er	—	1·20	1·06	—	1·35	0·70
Yb	—	1·32	1·06	—	1·39	0·73

No.—inclusion number. Trace elements in inclusions O-32 and Op-9 were analysed by proton microprobe, and those in other inclusions by ion microprobe.

parental melt compositions were calculated from whole-rock compositions using the method of Sobolev *et al.* (1993) for olivine-phyric rocks. The essence of this method is (1) calculation of groundmass composition on the basis of mass balance: groundmass + average olivine = rock (assuming equilibrium of the groundmass with the least magnesian olivine phenocryst), and (2) calculation of the parental composition by modelling the reverse of olivine fractional crystallization from the groundmass composition up to the moment of equilibrium with the most magnesian olivine found. Olivine–liquid equilibria were calculated using the model of Ford *et al.* (1983). The Fe^{2+}/Fe^{3+} value in melts was calculated using correlations between composition of spinel inclusions and host olivines (Fig. 2a) and the model of Maurel & Maurel (1982a) for Fe^{2+}/Fe^{3+} distribution in spinel and equilibrium melt (see Table 6 for equations). Additionally, this calculation for sample 5-25 was performed directly from the groundmass composition reported by Falloon *et al.* (1989), and for sample 26-2 from
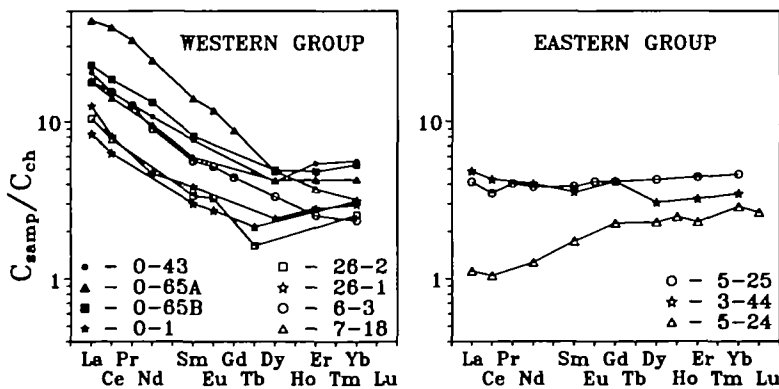

FIG. 6. Chondrite-normalized REE patterns of whole rocks (open symbols) and melt inclusions in olivines (filled symbols) from Tongan high-Ca boninite. Inclusions O-43, O-65A, and O-65B are from sample 26-2; inclusion O-1 is from sample 26-1. Normalization values are given in Table 3.

TABLE 6

Calculated parental and primary melts

Locality	Western group								Eastern group			
No.	1				2				3			
	Av.	S.D.	Max.	Min.	Av.	S.D.	Max.	Min.	Av.	S.D.	Max.	Min.
SiO_2	53·1	0·9	54·2	51·8	52·1	0·8	53·2	50·8	51·4	0·4	51·8	50·9
TiO_2	0·33	0·09	0·43	0·19	0·30	0·08	0·39	0·17	0·18	0·07	0·28	0·12
Al_2O_3	9·2	0·4	9·6	8·5	8·4	0·3	8·8	7·7	7·6	0·7	8·5	7·0
Fe_2O_3	1·0	0·1	1·1	0·9	0·9	0·1	1·0	0·9	0·9	0·02	0·9	0·9
FeO	7·8	0·4	8·6	7·3	7·7	0·4	8·4	7·2	8·4	0·2	8·5	8·1
MnO	0·2	0·04	0·24	0·11	0·1	0·04	0·22	0·10	0·2	0·02	0·18	0·14
MgO	19·2	1·0	21·1	18·2	21·9	1·2	23·9	20·9	24·0	0·6	24·6	23·3
CaO	7·7	0·5	8·2	6·8	7·0	0·4	7·5	6·2	6·4	0·1	6·6	6·3
Na_2O	1·1	0·16	1·3	0·9	1·0	0·15	1·2	0·8	0·8	0·17	1·0	0·6
K_2O	0·45	0·12	0·60	0·25	0·41	0·11	0·55	0·23	0·15	0·07	0·27	0·10
P_2O_5	0·10	0·08	0·22	0·05	0·10	0·08	0·20	0·05	0·02	0·01	0·03	0·01
H_2O	1·3	0·2	1·1	1·6	1·2	0·2	1·0	1·4	1·7	0·25	2·0	1·3
Fo	93·0				94·0				94·0			
T_{dry} (°C)	1420				1455				1485			
T_{cr} (°C)	1315–1325				1340–1360				1390			
P_{cr} (kbar)	0·4–0·9				0·4–0·9				0·9–1·7			
T_m (°C)					1440–1510				1540			
P_m (kbar)					20–25				25			

1—Western group parental melt (statistics for seven estimations); 2—Western group parental/primary melt (statistics for five estimations). Av.—average composition; 3—Eastern group parental/primary melt (statistics for seven estimations). Av.—average composition; Fo—composition of liquidus olivine; T_{dry}—calculated 1-atm dry olivine liquidus temperature (Ford et al., 1983); T_{cr}—liquidus temperature estimated from the experimental study of melt inclusion; P_{cr}—pressure of the beginning of crystallization; T_m—temperature of the last equilibrium with the mantle source; P_m—pressure of the last equilibrium with the mantle source. Estimations of primary melt for the Western and the Eastern group were calculated using the following correlations between Fe^{2+}/Fe^{3+} value in melt and liquidus olivine composition: $Fe^{2+}/Fe^{3+} = 0.436$ Fo $- 31.78$ and $Fe^{2+}/Fe^{3+} = 0.475$ Fo $- 34.09$, respectively.

compositions of homogenized melt inclusions in magnesian olivine. All these calculations assume that Fe–Mg partitioning between olivine and melt is independent of the presence of H_2O at the level of a few weight per cent, as was demonstrated by Ulmer (1989). The results obtained are shown in Table 6. Temperatures obtained via these calculations (T_{dry}, Table 6) correspond to equilibrium of these melts with olivine for 'dry' conditions.

Each group is characterized by a relatively narrow range of variation of major elements (SiO_2, Al_2O_3, FeO^*, MgO, and CaO). Standard deviations for these elements are apparently within total errors of the technique used. In contrast, relatively incompatible elements (TiO_2, Na_2O, K_2O, and P_2O_5) show a very large range, reflecting differences in primary melts.

The H_2O contents of parental melts were estimated using ion-probe data on the melt inclusions in high-Fo olivines from both groups of Tongan boninites (Table 4). The measured H_2O contents of these inclusions were corrected for olivine crystallization by a least-squares method (Wright & Doherty, 1970) using major-element compositions (SiO_2, Al_2O_3, FeO^*, MgO, and CaO) of the average parental magmas (Table 6). The results from both unheated inclusions and inclusions quenched after high-temperature experiments are similar for the Western group. The absolute values of H_2O content in the Eastern group lavas are significantly higher than those for the Western group, in striking contrast to the behaviour of other incompatible elements.

Primary melt compositions

A requirement of any established parental melt to be primary is that it has a high Mg_N (> 70), to be in equilibrium with mantle olivine (Green, 1970). However, the wide range of mantle olivine compositions (Fo_{94-87}) precludes the use of this criterion in quantitative calculations. Arai (1987, 1990) has shown that the olivine–spinel liquidus assemblage of mantle-derived primitive melts allows the correlation between compositions of coexisting olivines and spinels in the mantle to be used as a suitable criterion of primary magma candidacy (Fig. 7). The existence of such a correlation was shown theoretically [and experimentally by Jaques & Green (1980)] to result from mantle depletion owing to progressive partial melting.

The most primitive olivine–spinel associations observed in boninite and boninite-like magmas fall within the mantle array (Fig. 7), indicating possible equilibrium of parental melts with the mantle. To apply this criterion, however, it is necessary to know, and take into account, the dependence of mineral compositions in the liquidus assemblage on temperature and pressure, because the generation and crystallization of a melt are characterized by different P,T conditions (Appendix B). Available data show a small increase of olivine Mg_N with decreasing temperature (~ 0.5 Mg_N per $100\,°C$ for $T > 1300\,°C$) and its independence from pressure, and an increase of spinel Cr_N with decreasing pressure (10–15% in the range 15–1 kbar in the boninitic compositional range) and its independence of temperature. Using these estimations, it is possible to predict the change in composition of the primary liquidus assemblage with changing pressure if the magma P–T path is known. The latter can easily be obtained from numerous data on the olivine-saturated liquidus slope for high-Mg magmas ($\sim 5\,°C$/kbar, Ford et al., 1983). These calculations show that the slope of the shift in the Fo–Cr_N plot for the liquidus assemblage of derived parental melts is close to that of the mantle array (Fig. 7). Thus, despite a significant potential difference between temperature and pressure of melt segregation and crystallization, liquidus assemblages of parental melts can be used as a criterion of mantle origin.

The most primitive liquidus assemblage for the Eastern group plots at the magnesian border of the mantle array, implying that observed olivine Fo_{94} can be regarded as liquidus
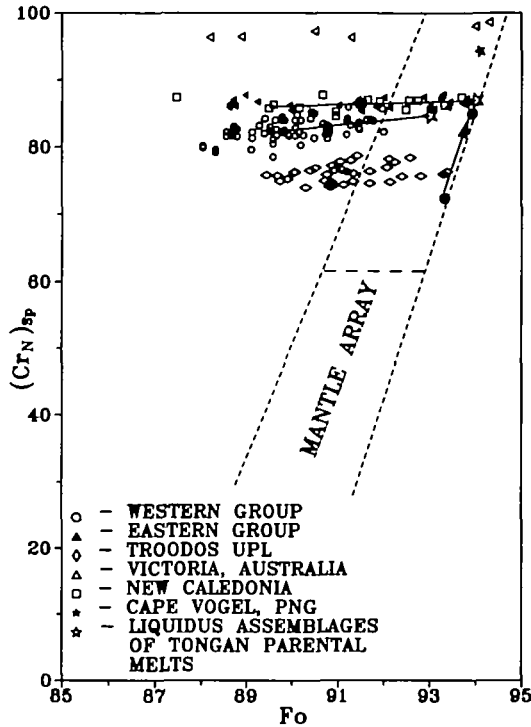
FIG. 7. Comparison of olivine–spinel liquidus association of high-Ca boninites with the Mantle Array (Arai, 1990). Cape Vogel, Papua New Guinea, data from Walker & Cameron (1983), Victoria data from Crawford (1980), New Caledonia data are our unpublished data; Troodos UPL data from Sobolev et al. (1993). ●, estimated shift in a liquidus assemblage composition (Fo$_{94}$, Cr$_N$=85) during 15 kbar ascent to the surface. (See text for discussion.) Horizontal dashed line indicates approximate border between lherzolites and harzburgites (Arai, 1987).

olivine for the primary melt for this suite and, correspondingly, that the established parental melt is identical to the primary melt. The most primitive liquidus assemblage of boninites from New Caledonia, Cape Vogel, and Victoria, and of Troodos Upper Pillow Lavas (UPL) also plot at the magnesian border of the mantle array, suggesting that it is a general feature of boninites. In contrast, the most primitive liquidus assemblage of the Tongan Western group has significantly less magnesian olivine for the corresponding spinel. This implies that more magnesian liquidus olivines (up to Fo$_{94}$) are likely to have been present in these suites, but are not recorded in studied samples. Thus we assume that the primary melt of the Western group boninites was in equilibrium with olivine Fo$_{94}$. The primary melt composition was calculated from the parental melt by modelling of reverse olivine fractional crystallization (Table 6).

H$_2$O contents of primary melts

The established degassing of Tongan boninites during crystallization raises the question of whether the H$_2$O content of Tongan primary melts can be derived from that of parental melts, or whether some H$_2$O was lost before crystallization began. As H$_2$O content was measured directly in melt inclusions in Fo$_{94}$ olivines from Eastern group lavas, the potential H$_2$O loss by degassing is limited, as H$_2$O decreases crystallization temperature. Therefore, an olivine-saturated melt should crystallize immediately after H$_2$O loss. However, H$_2$O loss
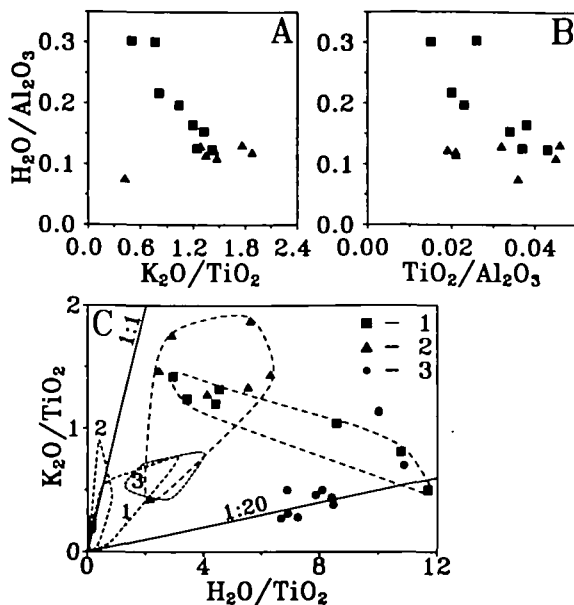
FIG. 8. A, B, correlation between H_2O and other incompatible elements in melt inclusions in high-magnesian olivines from Tongan high-Ca boninites. Absence of any correlation in Tongan glasses demonstrates their degassed nature. C, H_2O and K_2O contents in natural quenched glasses and melt inclusions from lavas of various tectonic settings. Normalization to TiO_2 used to avoid effects of crystallization. 1, Tongan boninite melt inclusions in high-magnesian olivines; 2, Tongan boninite glasses; 3, Troodos UPL glasses (Sobolev et al., 1993). Fields in C: 1, back-arc basin glasses; 2, MORB glasses; 3, arc tholeiites glasses; solid field, Hawaiian glasses. All data are from Danyushevsky et al. (1993) and reference therein.

before crystallization is still possible if the melt was superheated during ascent. Estimation of this effect is not quantitative at present, owing to lack of experimental data for ultramafic melts. Therefore, an independent criterion must be used to prove whether data obtained for parental melts are valid for primary melts. Correlation between H_2O and other incompatible element contents could be used as such a criterion. Figure 8 presents data on H_2O in melt inclusions in high-Fo olivines and glasses in the form of incompatible element ratios, to avoid effects of olivine and pyroxene fractionation. A significant difference between glasses and melt inclusions is obvious. Whereas glasses have nearly constant H_2O/Al_2O_3 values independent of variations in other incompatible element ratios, inclusions show a strong correlation of these parameters. Such systematic H_2O behaviour in melt inclusions indicates that they are relatively undegassed. Thus, H_2O contents of these inclusions may be taken as an estimation of H_2O contents in primary melts (Table 6).

Trace-element contents of primary melts

Chemical features of Tongan boninites suggest that a set of primary melts with distinctly different incompatible element contents but close major-element composition was involved in the formation of each suite. Therefore, we have calculated incompatible element contents in the primary melt from each individual whole-rock or melt-inclusion analysis. The procedure used involved addition/subtraction of a certain amount of olivine as determined by a least-squares mixing calculation method (Wright & Doherty, 1970). Contents of SiO_2, Al_2O_3, FeO^*, MgO, and CaO only were used in calculations. K_D values for all incompatible elements between olivine and melt were assumed equal to zero. Results are listed in Table 7.

TABLE 7

Calculated incompatible element contents in various Tongan boninite primary melts

Group	Western									Eastern		
Sample	26-1	0-1	26-2	0-32	0-43	0-65a	0-65b	6-3	7-18	5-24	5-25	3-44
Cs	0·14	—	0·18	—	—	—	—	—	—	—	—	—
Rb	4·77	—	9·17	7·22	7·85	6·08	6·02	6·69	9·93	1·79	2·33	4·46
Ba	49·4	—	99·1	81·8	—	—	—	87·9	190	30·5	31·9	78·7
Th	0·50	—	1·01	—	—	—	—	0·95	2·00	0·22	—	0·36
U	0·14	—	0·25	—	—	—	—	—	—	—	—	—
Ta	0·19	—	0·41	—	—	—	—	—	0·74	—	—	—
Nb	—	2·88	—	5·06	5·36	5·92	7·41	6·69	13·2	—	—	—
K	2049	1649	3832	3898	3256	3434	3310	2987	4879	1041	1031	2157
La	2·61	3·14	5·88	—	7·18	5·30	6·78	5·46	13·2	0·37	1·17	1·31
Ce	5·13	5·27	11·4	—	14·0	11·0	14·3	12·3	31·2	0·90	2·59	3·04
Pr	—	—	—	—	—	—	—	1·45	3·71	—	0·43	—
Sr	83·4	58·0	134	129	123	132	149	133	288	41·2	52·8	112
P	223	—	403	—	334	—	—	255	940	39·1	135	97·3
Nd	—	2·27	—	—	7·26	5·44	7·63	5·32	14·3	0·81	2·11	2·12
Zr	20·4	19·0	40·0	27·2	23·0	24·3	31·7	26·8	43·9	4·47	15·5	8·90
Hf	0·42	—	0·73	—	—	—	—	0·78	1·41	0·30	—	0·45
Sm	0·59	0·61	1·21	—	1·68	1·11	1·52	1·09	2·67	0·36	0·69	0·61
Eu	0·20	—	0·44	—	—	—	—	0·38	0·84	—	0·28	—
Ti	1123	1093	1846	2490	1773	1829	1856	1554	2234	806	1675	892
Gd	—	—	—	—	—	—	—	1·13	2·22	0·62	0·99	0·94
Tb	0·11	—	0·15	—	—	—	—	—	—	—	—	—
Dy	—	0·63	—	—	1·51	1·31	1·52	1·06	1·52	0·78	1·26	0·86
Y	5·96	3·69	9·23	—	—	—	—	6·69	9·11	4·48	7·76	5·20
Er	—	0·47	—	—	1·29	0·86	0·98	0·53	0·77	0·51	0·85	0·59
Yb	0·66	0·50	0·97	—	1·33	0·86	1·07	0·49	0·65	0·64	0·88	0·64

See text for calculation details.

P,T conditions of primary-melt formation and crystallization

The demonstrated saturation of primitive melts by an H_2O-rich fluid allows calculation of crystallization pressure, which is estimated from melt H_2O content using the Burnham (1979) model. Results for melt inclusions in high-Fo olivines are 0·4–0·9 kbar for the Western group lavas and 0·9–1·7 kbar for the Eastern group. These estimates correspond to the beginning of crystallization.

Crystallization temperature for the Western group primary melts can be extrapolated from the experimentally derived correlation between crystallization temperature and olivine composition (Fig. 5b). Only Fo–T pairs for runs with minimum temperature (see Table 4) were used to establish the Fo–T regression: T (°C) = (23·84 × Fo) − 903, which gives 1340 °C for Fo_{94}. This value is significantly lower than calculated 'dry' temperatures for this composition (Table 6), consistent with the presence of H_2O in these melts. The crystallization temperature can be also estimated from the difference between the measured and calculated 'dry' temperatures for homogenized melt inclusions in magnesian olivines (Danyushevsky *et al.*, 1992). The maximum difference determined, 95 °C, is the most reliable because of the demonstrated degassing of Tongan boninites during crystallization and possible H_2O loss during experiments in some runs (Appendix A). The result of such an estimation is 1360 °C, and 1340–1360 °C was accepted as the crystallization temperature for primary melts of the Western group (Table 6). Crystallization temperature of the Eastern group primary melt (1390 °C) was estimated from the 'dry' temperature and a correction (95°C) for H_2O content, obtained for the Western group melts (Table 6). This estimate is the maximum value, because H_2O content in the Eastern group melts is higher than in the Western group (Table 6).

Pressure of the last equilibrium of primary melts with their mantle sources was estimated using an approach originally proposed for 'dry' melting conditions by Jaques & Green (1980) and Takahashi & Kushiro (1983) and developed by Falloon & Green (1987, 1988) and Sobolev *et al.* (1992) (Fig. 9). The shift of isobars in this projection owing to the presence of 2 wt.% H_2O in the melt was estimated using experimental data of Green (1973, 1976) and Kushiro (1989, 1990). Results are shown in Table 6. Temperatures of primary melts segregation (Table 6) were calculated from established crystallization temperatures corrected for their pressure of formation, assuming an olivine-saturated liquidus $P–T$ slope of ~5 °C/kbar (Ford *et al.*, 1983).

DISCUSSION

MgO content of high-Ca boninite primary melts

One of the principal results of this study is a demonstration of very high MgO contents (21–24 wt.% MgO) of primary melts of Tongan high-Ca boninites. Similar high MgO contents have been also proposed for primary magmas of Troodos UPL (Sobolev *et al.*, 1993), which are another example of a high-Ca boninite suite, and for Cape Vogel (Walker & Cameron, 1983) and Victorian (Crawford, 1980) low-Ca boninites. However, our results are somewhat more magnesian than those estimated by Falloon & Green (1986) for primary melts of Tongan boninites (~17 wt.% MgO). The reason for this discrepancy for Tongan boninites is that Falloon & Green (1986) calculated the primary melt from the composition of naturally quenched melt inclusions in olivine Fo_{94}, which very likely have undergone a significant loss of iron after trapping. As we have shown, iron loss in inclusions is a widespread process for Tongan boninites and is explained by re-equilibration of inclusions with host olivine after trapping. As Falloon & Green (1986) derived their primary magma
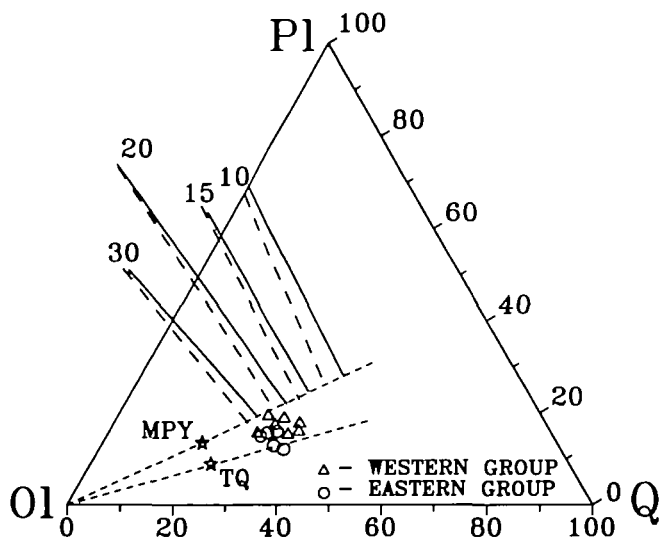
FIG. 9. Pressure of formation of Tongan high-Ca boninite primary melts. Walker-type (Walker *et al.*, 1979) projection from diopside apex. $Pl = Al_2O_3 + Na_2O + K_2O$, $Ol = (FeO + MgO + MnO + Al_2O_3 - CaO - Na_2O - K_2O - TiO_2 - Cr_2O_3)/2$, $Q = SiO_2 - [Al_2O_3 + FeO + MnO + MgO + 3 CaO + 11(Na_2O + K_2O) - TiO_2 - Cr_2O_3]/2$. Dashed lines—ol + opx ± cpx cotectics for dry mantle melting after Sobolev *et al.* (1992); solid lines—approximate position of these cotectics for 2 wt.% H_2O in melt (see text for references). MPY—composition of MORB pyrolite less 40% olivine (Falloon & Green, 1987); TQ—composition of Tinaquillo lherzolite less 40% olivine (Falloon & Green, 1988).

composition from a modified melt inclusion with an unrealistically low FeO/MgO value (Fig. 4), and calculated this up to equilibrium with olivine Fo_{94}, their primary magma has a significantly lower MgO content than our calculated 21–24 wt.%.

H_2O content of primary high-Ca boninite melts

The H_2O contents in the primary Tongan melts (from 1·1 to 2·0 wt.%) are among the first direct estimates for primary boninite melts. They are close to similar estimates for Troodos UPL primary melts (Sobolev *et al.*, 1993) and are in the range of those proposed for Western Pacific boninites on the basis of geochemical studies (Walker & Cameron, 1983; Dobson & O'Neil, 1987). Particularly significant is the demonstrated undegassed nature of these H_2O contents. Our estimates are significantly lower than those proposed for various primary boninite melts on the basis of recent experimental studies (Umino & Kushiro, 1989; Van der Laan *et al.*, 1989, and references therein). The reason for this overestimation of H_2O content in the latter studies is that relatively evolved samples were used as starting compositions for experimental runs. Underestimation of the normative olivine content of the starting compositions leads to overestimation of H_2O pressure necessary to produce olivine on their liquidus (Kushiro, 1972).

Our data suggest significantly H_2O-undersaturated conditions for generation of primary high-Ca boninite melts in the mantle. However, it is emphasized that these values are among the highest estimated for various mantle-derived magmas (Fig. 8C).

Temperature of primary high-Ca boninite melts and nature of their mantle source

Both the high MgO and relatively low H_2O contents established for primary high-Ca boninite magmas suggest exceptionally high temperatures for their origin. These values

(1400–1550 °C) are close to similar estimates for Troodos UPL primary melts (Sobolev *et al.*, 1993) and far exceed those proposed previously for boninites [up to 1350 °C, Crawford *et al.* (1989)]. These are critical for distinguishing between alternative scenarios of boninite generation, the nature of the high-Ca boninite mantle source, and the nature of interaction between the H_2O-bearing component and mantle source.

Postulated temperatures of primary high-Ca boninite melt formation strongly suggest that their mantle source is too hot to be a MORB mantle reservoir (Falloon & Green, 1987, 1988; McKenzie & Bickle, 1988; Sobolev & Dmitriev, 1989). Such temperatures occur in mantle with normal oceanic geotherms at the depths corresponding to the lower mantle [deeper than 700 km, e.g. Richter & McKenzie (1981)], and, if no major heating of diapirs occurs at shallow levels (unlikely, in our opinion), the high-Ca boninite source mantle must have originated from these depths. The temperature of the high-Ca boninite source is close to that of the OIB mantle reservoir, for which the same deep origin has been proposed (Wyllie, 1988; McKenzie & O'Nions, 1991). Refractory peridotite residual after extraction of plume-related melts could be the source of high-Ca boninites. In this framework, our data strongly suggest that primary high-Ca boninite melts are produced by melting an initially dry and hot source, triggered by introduction of some H_2O-bearing component(s).

Number and composition of components involved in high-Ca boninite petrogenesis

A number of established features of primary high-Ca boninite melts, including their location on an Ol–Q–Pl projection (Fig. 9) (which argues for a source more refractory than that of MORB), the composition of their primary liquidus assemblage (olivine Fo_{94}, spinel $Cr_N = 87$), and their low Ti contents, imply that the composition of their mantle source was significantly depleted. High CaO/Al_2O_3 values of primary melts (0·81–0·83) argue for clinopyroxene in the mantle source (Falloon *et al.*, 1989). Falloon & Crawford (1991) have inferred that the mantle source of these melts was a depleted lherzolite, consistent with data obtained here. The mantle residue after extraction of these melts is harzburgite. Formation of these melts via melting of a depleted lherzolite is shown in Fig. 9, where all estimations of primary melts lie above an olivine control line that passes through Tinaquillo lherzolite [see Falloon & Green (1987) for detailed discussion].

Despite this refractory source, the presence of strongly incompatible-element-enriched primary melts among high-Ca boninites, and their high H_2O contents, indicate that in addition to depleted lherzolite (referred to herein as component D), incompatible-element-enriched component(s) took part in their petrogenesis. Increasing absolute contents of the most incompatible elements (we have used La) lead to increases of La/K, La/Rb, La/Ba, La/Th, Ce/Sr, Sm/Hf, and Eu/Ti values for both groups of Tongan boninites (Fig. 10). These trends may be explained by mixing between two end-members. The first end-member (component E1), characterized by very low LREE contents, has low LREE/LILE values and is best represented by the composition of sample 5-24. The correlation between calculated La and K/Ti values in primary melts together with the strong inverse correlation between H_2O/Al_2O_3 and K/Ti (Fig. 8) argue that this component has a high H_2O content relative to the second end-member, as all primary Tongan boninite melts have similar Al_2O_3 contents. The second end-member (component E2) is characterized by high LREE, high La/Sm and La/Yb, and strong relative depletion in Zr, Hf, and Ti. It is best represented by sample 7-18.

Thus, the geochemical features of the Tongan high-Ca boninites can be explained by the interaction of an incompatible-element-depleted mantle source with two independent incompatible-element-enriched components. Geochemical features of the mantle source itself are probably reflected by middle to heavy REE contents in most LREE-depleted
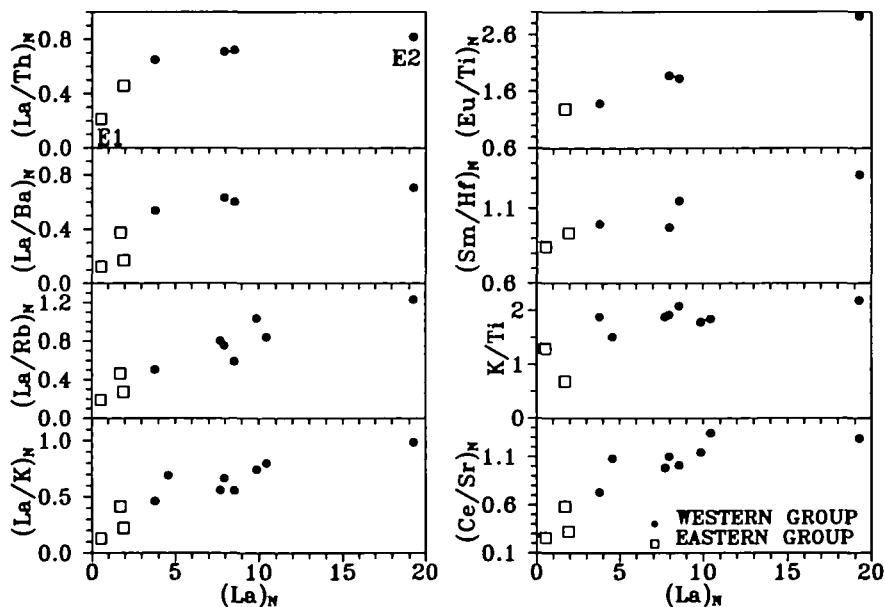
FIG. 10. Incompatible-element contents in primary Tongan high-Ca boninite melts. E1 and E2 represent two incompatible-element-enriched components involved in their petrogenesis (see text for discussion). Normalization to primitive mantle (Table 3).

primary melts. However, these could be affected by REE from component E1, concentrations of which are difficult to estimate at present. Component E1 contained mainly H_2O, LILE, and Th; H_2O/K_2O values in this component are ~ 20 (Fig. 8C), resembling Troodos UPL, and are the highest known for mantle-derived melts. High $H_2O/LILE$ values together with high LILE/REE values of this component indicate that it may be a fluid derived from a subducted slab. Our data suggest that the composition of this component in Tongan and Troodos boninites was essentially the same.

Component E2 was most likely an incompatible-element-enriched silicate melt. The presence of this component is a diagnostic feature of Tongan boninites, and those with a significant contribution of this component have lower H_2O contents than others, suggesting that it contains a relatively low H_2O content. This suggests, in turn, that it may not be related to subduction processes. Falloon & Crawford (1991) suggested, on the basis of isotope geochemistry and incompatible-element ratios, that this component could be an OIB-like melt, which is generally consistent with our data. Involvement of an incompatible-element-enriched silicate melt in Troodos UPL petrogenesis has been also demonstrated by Rogers *et al.* (1989) and Sobolev *et al.* (1993).

Our geodynamic model for the origin and interaction of components D, E1, and E2 will be published elsewhere (Danyushevsky *et al.*, in prep.).

CONCLUSIONS

(1) Primary high-Ca boninite melts from Tonga are characterized by high MgO contents (22–24 wt.%), and originated in a mantle wedge above a subduction zone at 20–25 kbar and 1450–1550 °C.

(2) H_2O contents in the primary melts vary from 2·0 to 1·3 wt.% for the Eastern group, and from 1·4 to 1·0 wt.% for the Western group.

(3) The primary melts crystallized in the presence of an H_2O-rich fluid in the temperature range 1390–1150 °C and pressures 1·7–0·15 kbar for the Eastern group and 0·9–0·3 kbar for the Western group.

(4) The data suggest that three independent components are involved in Tongan high-Ca boninite petrogenesis. Component D was a refractory mantle depleted in incompatible elements, likely to be hot 'dry' lherzolite produced by previous melting with a mantle plume. Component E1 was an H_2O-rich fluid containing LILE and Th, which has an H_2O/K_2O value of 20 and was produced by dehydration of a subducted slab. Component E2 is thought to be an incompatible-element-enriched silicate melt of plume origin.

(5) Primary high-Ca boninite primary melts form as a result of interaction between hot dry mantle and H_2O-bearing subduction-related fluid.

REFERENCES

Arai, S., 1987. An estimation of the least depleted spinel peridotite on the basis of olivine–spinel mantle array. *Neues Jahrb. Miner. Monatsh.* **8**, 347–54.

—— 1990. What kind of magma could be equilibrated with ophiolitic peridotites? In: Malpas, J., Moores, E. M., Panayiotou, A., & Xenophontos, C. (eds.) *Ophiolites.* Nicosia: Cyprus Geological Survey, 557–84.

Bakumentko, I. T., 1975. Inclusions in minerals of ultrabasic nodules as indicators of their origin. In: Sobolev, V. S., Dobretsov, N. L., & Sobolev, N. V. (eds.) *Deepseated Xenoliths of the Upper Mantle.* Novosibirsk: Nauka (Siberian Branch), 231–5 (in Russian).

Bloomer, S. H., & Hawkins, J. M., 1987. Petrology and geochemistry of boninite series volcanic rocks from the Mariana Trench. *Contr. Miner. Petrol.* **97**, 361–77.

Burnham, C. W., 1979. The importance of volatile constituents. In: Yoder, H. S. (ed.) *Evolution of Igneous Rocks.* Princeton, NJ: Princeton University Press, 439–82.

—— Davis, N. F., 1974. The role of H_2O in silicate melts: II. Thermodynamic and phase relations in the system $NaAlSi_3O_8$–H_2O to 10 kb. *Am. J. Sci.* **274**, 902–40.

Cameron, W. E., 1985. Petrology and origin of primitive lavas from the Troodos ophiolite, Cyprus. *Contr. Miner. Petrol.* **89**, 239–55.

—— 1989. Contrasting boninite–tholeiite associations from New Caledonia. In: Crawford, A. J. (ed.) *Boninites and Related Rocks.* London: Unwin Hyman, 314–38.

—— McCulloch, M. T., & Walker, D. A., 1983. Boninite petrogenesis: chemical and Nd–Sr isotopic constraints. *Earth Planet. Sci. Lett.* **65**, 75–89.

Chayla, B., Jaffrezic, H., & Joron, J.-L., 1973. Analyse par activation dans les neutrons épithermiques. Application à la détermination d'éléments en trace dans les roches. *C. R. Acad. Sci. Paris* **277**, 273–5.

Clocchiatti, R., 1975. Les inclusions vitreuses du quartz: données optiques, thermométriques et chimiques. *Mém. Soc. Géol. Fr.* **284**, 2203–6.

Crawford, A. J., 1980. A clinoenstatite-bearing cumulate olivine pyroxenite from Howqua, Victoria. *Contr. Miner. Petrol.* **75**, 353–67.

—— Cameron, W. E., 1985. Petrology and geochemistry of Cambrian boninites and low-Ti andesites from Heathcote, Victoria. *Ibid.* **91**, 93–104.

—— Falloon, T. J., & Green, D. H., 1989. Classification, petrogenesis and tectonic setting of boninites. In: Crawford, A. J. (ed.) *Boninites and Related Rocks.* London: Unwin Hyman, 1–49.

Danyushevsky, L. V., Falloon, T. J., Sobolev, A. V., Crawford, A. J., Carroll, M., & Price, R. C., 1993. The H_2O content of basalt glasses from South West Pacific back-arc basins. *Earth Planet. Sci. Lett.* **117**, 347–62.

—— Sobolev, A. V. & Kononkova, N. N., 1992. Methods of studying magma inclusions in minerals during investigations on water-bearing primitive mantle melts (Tonga trench boninites). *Geochem. Int.* **29**, 48–62.

Dobson, P. F., & O'Neil, J. R., 1987. Stable isotope compositions and water content of boninite series volcanic rocks from Chichi-jima, Bonin Islands, Japan. *Earth Planet. Sci. Lett.* **82**, 75–86.

Falloon, T. J., & Crawford, A. J., 1991. The petrogenesis of high-calcium boninites from the north Tonga ridge. *Ibid.* **102**, 375–94.

—— Green, D. H., 1986. Glass inclusions in magnesian olivine phenocrysts from Tonga: evidence for highly refractory parental magmas in the Tonga arc. *Ibid.* **81**, 95–103.

—— —— 1987. Anhydrous partial melting of MORB pyrolite and other peridotite compositions at 10 kb: implications to the origin of primitive MORB glasses. *Miner. Petrol.* **37**, 181–219.

—— —— 1988. Anhydrous partial melting of peridotite from 8 to 35 kb and the petrogenesis of MORB. *J. Petrology*, Special Lithosphere Issue, 379–414.

—— —— Crawford, A. J., 1987. Dredged igneous rocks from the northern termination of the Tofua magmatic arc, Tonga and adjacent Lau Basin. *Aust. J. Earth Sci.* **34**, 487–506.

—— —— Hatton, C. J., & Harris, K. L., 1988. Anhydrous partial melting of a fertile and depleted peridotite from 2 to 30 kb and application to basalt petrogenesis. *J. Petrology* **29**, 1257–82.

—— —— McCulloch, M. T., 1989. Petrogenesis of high-Mg and associated lavas from the North Tonga Trench. In: Crawford, A. J. (ed.) *Boninites and Related Rocks.* London: Unwin Hyman, 357–95.

Fisk, M. R., & Bence, A. E., 1980. Experimental crystallization of chrome spinels in FAMOUS basalt 527-1-1. *Earth Planet. Sci. Lett.* **48**, 111–23.

Ford, C. E., Russell, D. G., Groven, J. A., & Fisk, M. R., 1983. Distribution coefficients of Mg^{2+}, Fe^{2+}, Ca^{2+} and Mn^{2+} between olivine and melt. *J. Petrology* **24**, 256–65.

Fujii, T., & Scarfe, C. M., 1985. Composition of liquids coexisting with spinel lherzolite at 10 kb and the genesis of MORB. *Contr. Miner. Petrol.* **90**, 18–28.

Govindaraju, K., & Mevelle, G., 1987. Fully automated dissolution and separation methods for inductively coupled plasma atomic emission spectrometry rock analysis. *J. Anal. Atom. Spectrom.* **2**, 615–19.

Green, D. H., 1970. The origin of basaltic and nephelinitic magmas. *Trans. Leicester Lit. Phil. Soc.* **64**, 28–54.

—— 1973. Conditions of melting of basanite magma from garnet peridotite. *Earth Planet. Sci. Lett.* **17**, 456–65.

—— 1976. Experimental testing of 'equilibrium' partial melting of peridotite under water-saturated, high-pressure conditions. *Can. Miner.* **14**, 255–68.

Grove, T. L., & Bryan, W. B., 1983. Fractionation of pyroxene-phyric MORB at low pressure: an experimental study. *Contr. Miner. Petrol.* **84**, 293–309.

Grover, J. E., Lindsley, D. H., & Bence, A. E., 1980. Experimental phase relations of olivine vitrophyres from breccia 14321: the temperature- and pressure-dependence of Fe–Mg partitioning for olivine and liquid in a highlands melt-rock. In: Merrill, R. B. (ed.) *Proc. 11th Lunar Sci. Conf.* New York: Pergamon Press, 179–96.

Gurenko, A. A., Sobolev, A. V., & Kononkova, N. N., 1991. Petrology of the primary magma of the Reykjanes peninsula rift tholeiites. *Geochem. Int.* **28**, 58–71.

Hickey, R. L., & Frey, F. A., 1982. Geochemical characteristics of boninite volcanics: implications for their source. *Geochim. Cosmochim. Acta* **46**, 2099–115.

Jaques, A. L., & Green, D. H., 1980. Anhydrous melting of periodotite at 0–15 kb pressure and the genesis of tholeiitic basalts. *Contr. Miner. Petrol.* **73**, 287–310.

Jarosewich, E. J., Nelen, J. A., & Norberg, J. A., 1980. Reference samples for electron microprobe analyses. *Geostandards Newslett.* **4**, 257–8.

Kuroda, N., Shiraki, K., & Urano, H., 1978. Boninite as a possible calc-alkalic primary magma. *Bull. Volcanol.* **41**, 563–75.

Kushiro, I., 1972. Effect of water on the composition of magmas formed a high pressure. *J. Petrology* **13**, 311–34.

—— 1989. Generation and ascent of magma in island-arcs in relation to crustal growth. In: *28th Int. Geol. Congr. Abstr.*, **2**, 243.

—— 1990. Partial melting of mantle wedge and evolution of island-arc crust. *J. Geophys. Res.* **95B**, 15929–39.

Lavrentev, Yu. G., Pospelova, L. N., & Sobolev, N. V., 1974. Rock-forming mineral compositions determination by X-ray microanalysis. *Zavod. Lab.* **40**, 657–66. (in Russian).

Lindsley, D. H., 1983. Pyroxene thermometry. *Am. Miner.* **68**, 477–93.

Maurel, C., & Maurel, P., 1982a. Étude expérimentale de l'équilibre $Fe^{2+}-Fe^{3+}$ dans les spinelles chromifères et les liquides silicates basiques coexistants, à 1 atm. *C. R. Acad. Sci. Paris* **285**, 209–15.

—— —— 1982b. Étude expérimentale de la distribution de aluminium entre bain silicate basique et spinelle chromifère. Implications pétrogénétiques: teneur en chrome des spinelles. *Bull. Minér.* **105**, 197–202.

McKenzie, D., & Bickle, N. J., 198. The volume and composition of melt generated by extension of the lithosphere. *J. Petrology* **29**, 625–80.

—— O'Nions, R. K., 1991. Partial melt distributions from inversion of rare earth element concentrations. *Ibid.* **32**, 1021–91.

Meijer, A., 1980. Primitive arc volcanism and a boninite series: examples from western Pacific island-arcs. In: Hayes, D. E. (ed.) *The Tectonic and Geological Evolution of Southeast Asian Seas and Islands. Geophys. Monogr. Am. Geophys. Union* **23**, 271–82.

Nelson, S. A., & Carmichael, I. S. E., 1979. Partial molar volumes of oxide components in silicate liquids. *Contr. Miner. Petrol.* **71**, 117–24.

Nikogosian, I. K., 1990. Petrology and geochemistry of primary melts of tholeiitic and subalkaline suites from Hawaii and Reunion. Ph.D. Thesis, Vernadsky Institute of Geochemistry, Moscow, 305 pp. (in Russian).

Ohnenstetter, D., & Brown, W. L., 1992. Overgrowth textures, disequilibrium zoning, and cooling history of a glassy four-pyroxene boninite dyke from New Caledonia. *J. Petrology* **33**, 231–71.

Pearce, J. A., van der Laan, S. R., Arculus, R. J., Murton, B. J., Ishii, T., Peate, D. W., & Parkinson, I. J., 1992. Boninite and harzburgite from Leg 125 (Bonin–Mariana forearc): a case study of magma genesis during the initial stages of subduction. In: Fryer, P., Pearce, J. A., Stokking, L. B., et al. (eds.) *Proc. Ocean Drilling Program, Sci. Results, 125*. College Station, TX: Ocean Drilling Program, 623–62.

Peive, A. V. (ed.), 1980. *Geology of the Philippine Sea Floor.* Moscow: Nauka, 262 pp. (in Russian).

Richter, F. M., & McKenzie, D. P., 1981. On some consequences and possible causes of layered mantle convection. *J. Geophys. Res.* **86**, 6133–42.

Roedder, E., 1984. Fluid inclusions. *Miner. Soc. Am. Rev. Miner.* **14**, 620 pp.

Roeder, P. L., & Emslie, R. F., 1970. Olivine–liquid equilibrium. *Contr. Miner. Petrol.* **29**, 275–89.

Rogers, N. W., MacLeod, C. J., & Murton, B. J., 1989. Petrogenesis of boninitic lavas from the Limassol Forest Complex, Cyprus. In: Crawford, A. J. (ed.) *Boninites and Related Rocks.* London: Unwin Hyman, 288–313.

Sack, R. O., 1982. Spinels as petrogenetic indicators: activity–composition relations at low pressures. *Contr. Miner. Petrol.* **79**, 169–86.

Sharaskin, A. Ya., Karpenko, S. F., Ljalikov, A. V., Zlobin, S. K., & Balashov, Yu. A., 1983a. Correlated $^{143}Nd/^{144}Nd$ and $^{87}Sr/^{86}Sr$ data on boninites from Mariana and Tonga arcs. *Ofioliti* **8**, 431–8.

—— Putchin, I. K., Zlobin, S. K., & Kolesov, G. M., 1983b. Two ophiolite sequences from the basement of the Northern Tonga Arc. *Ibid.* **8**, 411–30.

Shimizu, N., & Hart, S. R., 1982. Application of the ion microprobe to geochemistry and cosmochemistry. *Ann. Rev. Earth Planet Sci.* **10**, 483.

Sie, S., H., Ryan, C. G., Cousens, D. R., & Suter, G. F., 1990. A tandetron-based microbeam system. *Nucl. Instrum. Meth. Phys. Res.* **B45**, 543–7.

Simkin, T., & Smith, J. V., 1980. Minor-element distribution in olivine. *J. Geol.* **78**, 304–35.

Sobolev, A. V., Clocchiatti, R., & Dhamelincourt, P., 1983. Les variations de la température et de la pression partielle d'eau pendant la cristallisation de l'olivine dans les océanites du Piton de la Fournaise (Réunion éruption de 1966). *C. R. Acad. Sci. Paris* **296**, 275–80.

—— Danyushevsky, L. V., 1986. Proof of the magmatic origin of water and its estimated concentration in residual boninite melt. *Trans. USSR Acad. Sci., Earth Sci.* **288**, 119–22.

—— Dmitriev, L. V., 1989. Primary melts of tholeiites of oceanic rifts (TOR): evidence from studies of primitive glasses and melt inclusions in minerals. *28th Int. Geol. Congr. Abstr.*, **3**, 147–8.

—— —— Barsukov, V. L., Nevsorov, V. N., & Slutsky, A. B., 1980. The formation conditions of the high-magnesian olivines from the monomineralic fraction of Luna 24 regolith. *Proc. 11th Lunar Sci. Conf.* 105–16.

—— Kamenetsky, V. S., & Kononkova, N. N., 1992. New data on Siberian meimechites petrology. *Geochem. Int.* **29**, 10–20.

—— —— Metrich, N., Clocchiatti, R., Kononkova, N. N., Devirts, A. L., & Ustinov, V. I., 1991. Volatile regime and crystallization conditions in Etna hawaiite lavas. *Ibid.* **28**, 53–65.

—— Portnyagin, M. V., Dmitriev, L. V., Tsamerian, O. P., Danyuskevsky, L. V., Kononkova, N. N., Shimizu, N., & Robinson, P. T., 1993. Petrology of ultramafic lavas and associated rocks of the Troodos Massif, Cyprus. *Petrology* **1**, 331–61.

Stern, R. J., Morris, J., Bloomer, S. H., & Hawkins, J. W., 1991. The source of the subduction component in convergent margin magmas: trace-element and radiogenic isotope evidence from Eocene boninites, Mariana forearc. *Earth Planet. Sci. Lett.* **55**, 1467–81.

Stolper, E., 1980. A phase diagram for mid-ocean ridge basalts: preliminary results and implications for petrogenesis. *Contr. Miner. Petrol.* **74**, 13–27.

Sun, S.-S., & McDonough, W. F., 1989. Chemical and isotopic systematics of oceanic basalts: implication for mantle composition and processes. In: Saunders, A. D., & Norry, M. J. (eds.) *Magmatism in the Ocean Basins. Geol. Soc. Spec. Publ.* **42**, 313–45.

Takahashi, E., & Kushiro, I., 1983. Melting of a dry peridotite at high pressure and basalt magma genesis. *Am. Miner.* **68**, 859–79.

Taylor, S. R., & McLennan, S. M., 1981. The composition and evolution of continental crust: rare earth element evidence from sedimentary rocks. *Phil. Trans. R. Soc. Lond.* **301A**, 381–99.

Ulmer, P., 1989. The dependence of the Fe^{2+}–Mg cation-partitioning between olivine and basaltic liquid on pressure, temperature and composition. An experimental study to 30 kbar. *Contr. Miner. Petrol.* **101**, 261–73.

Umino, S., & Kushiro, I., 1989. Experimental studies on boninite petrogenesis. In: Crawford, A. J. (ed.) *Boninites and Related Rocks.* London: Unwin Hyman, 89–111.

Van der Laan, S. R., Flower, M. F. J., & Koster van Groos, A. F., 1989. Experimental evidence for the origin of boninites: near-liquidus phase relations to 7·5 kbar. *Ibid.* 112–47.

Visotsky, S. V., 1989. *Ophiolite Assemblages of Pacific's Island-Arc Systems.* Vladivostok: Far East Branch Academy of Sciences of the USSR, 196 pp. (in Russian).

Walker, D., Shibara, T., & DeLong, S. E., 1979. Abyssal tholeiites from the Oceanographer fracture zone. II. Phase equilibria and mixing. *Contr. Miner. Petrol.* **70**, 111–25.

Walker, D. A., & Cameron, W. E., 1983. Boninite primary magmas: evidence from the Cape Vogel peninsula, PNG. *Ibid.* **83**, 150–8.

Wright, T. L., & Doherty, P. C., 1970. A linear programming and least squares computer method for solving petrologic mixing problems. *Geol. Soc. Am. Bull.* **88**, 95–115.

Wyllie, P. J., 1988. Solidus curves, mantle plumes and magma generation beneath Hawaii. *J. Geophys. Res.* **93B**, 4171–81.

APPENDIX A: INCLUSIONS IN MINERALS

Experimental study of melt inclusions

Theoretical aspects of melt and fluid inclusions study have been discussed by Roedder (1984). At room temperature, primary melt inclusions consist of several phases (i.e., quench glass, gas bubble, crystals), which precipitate during cooling owing to crystallization inside inclusions and thermal skrinkage. (Note that the host-mineral always crystallizes on the inclusion walls rather than as discrete crystals inside the inclusion volume, so inclusions at room temperature always consist at least of two phases—quenched glass and crystals on the walls.) The central point of melt inclusions practice is the homogenization of an inclusion. This is the moment of reverse transformation into a homogeneous melt which is fixed by the dissolution of the last phase inside an inclusion, which is normally a shrinkage gas bubble (Roedder, 1984). In the ideal case, for a gas-saturated system, the inclusion composition at this moment is equal to the composition of the trapped melt and the temperature of homogenization matches the temperature of trapping. In real cases, several problems arise as a result of kinetics of melting and behaviour of H_2O inside inclusions.
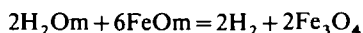
Kinetic effects on the temperature of homogenization

Kinetic problems (in our case, the relationship between rate of heating and rate of melting of crystalline phases within the inclusion volume and from inclusion walls) are well known in the literature. For melt inclusions, the dependence of homogenization temperature on heating velocity was shown by Bakumenko (1975). An increase of heating velocity in the high-temperature range (> 1100 °C) causes an exponential increase in the homogenization temperature, whereas its decrease causes an asymptotic decrease of the homogenization temperature to a constant value. This value is accepted as the true temperature of homogenization. The appropriate velocity in each case depends on the melt composition, the size of the inclusion, the temperature of the experiment, and the type of the host mineral. For ultramafic to basaltic compositions of the melt, the most suitable range of velocities is from 1 °C/s to 1 °C/min (Danyushevsky *et al.*, 1992). The dependence of suitable velocity on the inclusion size is shown in Fig. 5D for a MORB olivine from the Atlantic. The size increase of the inclusion leads to the necessity of decreasing the heating velocity, so that 40-μm and larger MORB inclusions in olivine should be heated significantly slower than 1 °C/min to obtain the true homogenization temperature. To choose the appropriate velocity in the high-temperature range it is necessary to carry out similar kinetic experiments in each case.

The above pertains to cases where exchange processes between an inclusion and its environment during the run are not significant. However, such cases are basically those where disssociation of H_2O inside inclusions is insignificant and the method of homogenization then allows establishment of the mineral crystallization temperatures with an accuracy of 10–20 °C. Determination of the composition of the quenched homogenized melt inclusion then allows determination of the composition of the melt with an accuracy of 5 rel.% for most major elements (e.g., Sobolev *et al.*, 1991).

The influence of H_2O dissociation

As was shown by Sobolev et al. (1983), in some cases a continuous increase of the homogenization temperature occurs at high temperatures ($> 1100\,°C$) during the run. This process is accompanied by precipitation of magnetite inside such inclusions and is explained by H_2 loss reactions such as

$$2H_2Om + 6FeOm = 2H_2 + 2Fe_3O_4$$

or

$$H_2Om + 2FeOm = H_2 + Fe_2O_3m \text{ (at temperatures higher than magnetite stability),}$$

which proceed owing to the strong diffusive ability of H_2 and the difference in its fugacity inside and outside the inclusion during the experiments. This difference occurs because runs are carried out at 1 atm external pressure of inert gas, whereas the pressure inside the inclusions is, in general, close to the pressure of trapping near homogenization temperature. The reaction is limited by the ability of the melt to oxidize. The main compound of natural melts which can be oxidized is Fe^{2+}. It is a simple calculation to determine the maximum amount of H_2O which may dissociate: H_2O (wt.%) = $0.125 \times C_{(FeO)}$, where $C_{(FeO)}$ = wt.% FeO in the melt. For basaltic melts, the maximum amount of 'lost' H_2O is < 1 wt.%. In acid melts, with FeO content < 2 wt.%, possible 'lost' H_2O contents are < 0.25 wt.% and so the effect must be minimal. Experimental data of Clocchiatti (1975) confirm this suggestion.

Two different effects will occur owing to H_2O dissociation: a volume reduction of melt as a result of disappearance of the component with large molar volume, and the known influence of H_2O on the temperature of melting. Both of these factors will change the homogenization temperature. Calculations using data of Nelson & Carmichael (1979) for molar volumes of major elements in melts and data of Burnham & Davis (1974) for molar volume of H_2O in albite melt show that, at low pressures (< 2 kbar) and at high temperatures ($> 1100\,°C$), the first factor is the most significant. This effect could have a dramatic influence on the homogenization temperature. As will be shown below, the homogenization temperature of small inclusions may increase by $150\,°C$ during the first few minutes of the run.

If pressure inside an inclusion is high during an experiment, this effect lessens, owing to the volume reduction of H_2O in melt (Burnham & Davis, 1974), and the second factor is the main one. This effect is pressure independent and comparatively small. For inclusions in olivine and clinopyroxene it does not exceed $40\,°C$ (if 1 wt.% H_2O dissociates). This means that under high-pressure conditions the homogenization temperature should not increase strongly. This suggestion is confirmed by experimental results of a study of melt inclusions trapped by minerals from alkaline Hawaiian suites at 5 kbar (Nikogosyan, 1990). During these experiments, the homogenization temperature increases only slightly, in spite of the H_2O dissociation which is confirmed by the appearance of magnetite.

In summary, the measurement of crystallization temperatures using the method of homogenization is relatively difficult for H_2O-bearing melts which crystallized at low pressures. Dissociation of H_2O can increase the homogenization temperature by more than $100\,°C$. However, the experimental study of hawaiite magmas from Etna volcano (Sobolev et al., 1991) which contain ~ 1 wt.% H_2O, shows that the use of the optimal experimental conditions, based on the kinetics experiments, makes it possible to establish the temperature of crystallization and the melt compositions with an accuracy close to that obtained for 'dry' melts. Independent criteria to test measured temperatures are necessary in each case.

Experiments with melt inclusions during this study

The experimental study of the melt temperatures in olivine and orthopyroxene from sample 26-2 was carried out using a high-T heating stage in an atmosphere of high-purity He under visual control. The heating stage has been described by Sobolev et al. (1980). Primary melt inclusions of homogeneous trapping were used for the experiments. During the runs, a rapid increase of the temperature of homogenization at high temperatures ($> 1100\,°C$), and magnetite crystallization in inclusions in orthopyroxenes were noted. Suitable experimental conditions involving appropriate heating velocity, run duration, and size of the inclusions were determined on the basis of 15 kinetics experiments summarized in Fig. 5C. Runs with olivine as host mineral were carried out under the following conditions: size of inclusions $100–150$ μm; duration of runs at high temperatures < 1 min, heating velocity near the homogenization temperature $30–40\,°C$/min. During runs with inclusions in orthopyroxene, these conditions were $50–70$ μm, $< 3–4$ min and $10–20\,°C$/min, respectively.

APPENDIX B: THE DEPENDENCE OF LIQUIDUS ASSEMBLAGE COMPOSITION OF A MELT ON PRESSURE AND TEMPERATURE

Olivine

Treatments of experimental data on equilibrium between olivine and dry melt at low pressures and temperatures below 1300 °C (e.g., Roedder & Emslie, 1970; Ford et al., 1983) suggest that K_D of Fe–Mg partitioning is independent of temperature. The data at higher pressures, and therefore at higher temperatures, show increasing K_D values, which are usually interpreted as the effect of pressure (Ford et al., 1983; Takahashi & Kushiro, 1983; Ulmer, 1989), but the possibility of the hidden effect of temperature has also been mentioned (Takahashi & Kushiro, 1983). To clarify the K_D behaviour, a statistical treatment of available data at high temperatures (> 1300 °C) was carried out. The following criteria were used for data selection:

(1) to avoid problems of quenching, only data from 'sandwich' and liquidus experiments were used;
(2) to be sure that the main form of Fe is FeO, only experiments in graphite or iron capsules were chosen;
(3) experiments were anhydrous.

Some 88 selected pairs (Grover et al., 1980; Stolper, 1980; Takahashi & Kushiro, 1983; Falloon & Green, 1987, 1988; Falloon et al., 1988) are plotted in Fig. B1.A, and show a significant positive correlation of K_D values with temperature and its near independence of pressure:

$$\ln(K_D) = -1541 \cdot 1/T(K) - 2 \cdot 3364 \times (P-1)/T(K) - 0 \cdot 1823 \ (P \text{ in bars}).$$

The correlation between K_D and temperature is

$$\ln(K_D) = -1624 \cdot 0/T(K) - 0 \cdot 1448 \quad (r = -0 \cdot 809)$$

or, in a more simple form,

$$K_D = 1 \cdot 853e - 4 \times T(°C) + 0 \cdot 069 \quad (r = 0 \cdot 811).$$

The result is the opposite of that obtained by Ulmer (1989), who argued for K_D independence of temperature. However, his data at high temperatures were obtained in the presence of unmeasured amounts of H_2O. Dissociation owing to the diffusion of hydrogen could significantly increase the oxygen fugacity in the melt and hence the Fe_2O_3 content, leading to a systematic decrease of K_D values. Because of this possible problem, we prefer to use 'dry' experiments in our treatment. We believe that the presence of small amounts of H_2O in the melt (2–3 wt.%) will not strongly affect the derived correlation.

Spinel

To estimate the effect of pressure and temperature on the composition of liquidus spinel, available data on compositions of coexisting melts and spinels were selected over a wide range of temperature
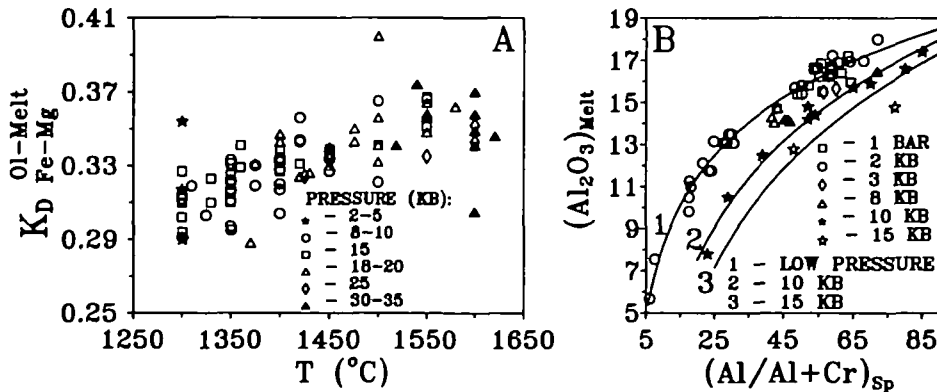

FIG. B1. A, correlation between K_D of Fe–Mg exchange between olivine and melt and the temperature of equilibria. B, pressure dependence of spinel composition in equilibrium with melt.

(1200–1400 °C), pressure (1 atm–15 kbar) and melt compositions (Fig. B1.B). Data from experiments and from melt inclusions in minerals were used. The data were divided into three groups: $P < 2$ kbar, $P = 10$ kbar and $P = 15$ kbar. The first group consists of experiments at 1 atm (Fisk & Bence, 1980; Sack, 1982; Grove & Bryan, 1983) and results of melt inclusion studies, in which pressure was determined independently by the study of fluid inclusions (Nikogosyan, 1990, and our data). The other two groups consist of data from Jaques & Green (1980) and Fujii & Scarfe (1985). In all cases, TiO_2 content in spinels were < 0.5 wt.%. Al_2O_3 content in melts was chosen as a melt composition indicator, because the experimental study of Maurel & Maurel (1982b) showed a strong positive correlation between Al_2O_3 content in coexisting spinels and melts. From Fig. B1.B, the decrease of Cr_N of spinel with increasing pressure is obvious.

Data from melt inclusion studies at 8 and 3 kbar (Nikogosyan, 1990; Gurenko et al., 1991) were used as independent criteria of the correlation obtained.